

Article

Synthesis and Application of Novel Ruthenium Catalysts for High Temperature Alkene Metathesis

Tegene T. Tole, Jean I. du Toit, Cornelia G. C. E. van Sittert, Johan H. L. Jordaan and Hermanus C. M. Vosloo *

Research Focus Area for Chemical Resource Beneficiation, Catalysis and Synthesis Research Group, North-West University, Hoffmann Street, 2531 Potchefstroom, South Africa; 24043036@nwu.ac.za (T.T.T.); 12317624@nwu.ac.za (J.I.d.T.); cornie.vansittert@nwu.ac.za (C.G.C.E.v.S.); johan.jordaan@nwu.ac.za (J.H.L.J.)
 * Correspondence: manie.vosloo@nwu.ac.za; Tel.: +27-18-299-1669

Academic Editors: Albert Demonceau, Ileana Dragutan and Valerian Dragutan

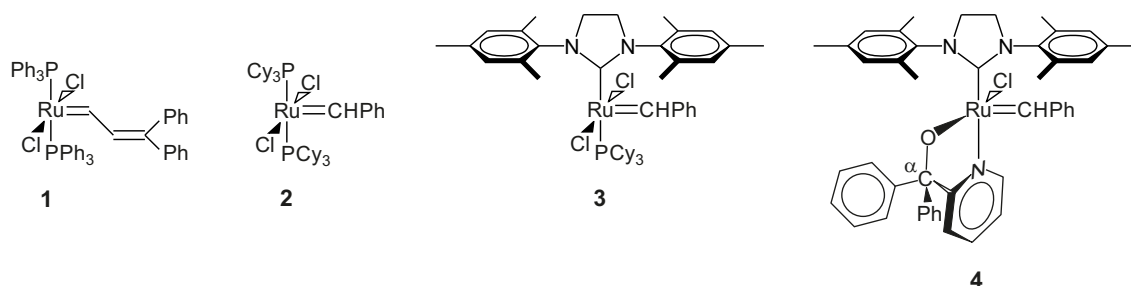
Received: 24 November 2016; Accepted: 3 January 2017; Published: 10 January 2017

Abstract: Four pyridinyl alcohols and the corresponding hemilabile pyridinyl alcoholato ruthenium carbene complexes of the Grubbs second generation-type $\text{RuCl}(\text{H}_2\text{IMes})(\text{O}^-\text{N})(=\text{CHPh})$, where $\text{O}^-\text{N} = 1-(2'\text{-pyridinyl})-1,1\text{-diphenyl methanolato}$, $1-(2'\text{-pyridinyl})-1-(2'\text{-chlorophenyl}), 1\text{-phenyl methanolato}$, $1-(2'\text{-pyridinyl})-1-(4'\text{-chlorophenyl}), 1\text{-phenyl methanolato}$ and $1-(2'\text{-pyridinyl})-1-(2'\text{-methoxyphenyl}), 1\text{-phenyl methanolato}$, are synthesized in very good yields. At high temperatures, the precatalysts showed high stability, selectivity and activity in 1-octene metathesis compared to the Grubbs first and second generation precatalysts. The 2-/4-chloro- and 4-methoxy-substituted pyridinyl alcoholato ligand-containing ruthenium precatalysts showed high performance in the 1-octene metathesis reaction in the range 80–110 °C. The hemilabile 4-methoxy-substituted pyridinyl alcoholato ligand improved the catalyst stability, activity and selectivity for 1-octene metathesis significantly at 110 °C.

Keywords: alkene metathesis; hemilabile ligand; pyridinyl alcohol; ruthenium carbene; Grubbs-type precatalyst; 1-octene

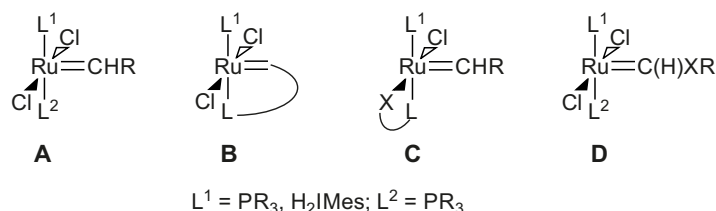
1. Introduction

The well-defined Grubbs first (1 and 2) [1–4] and second (3) [5–7] generation precatalysts are found to be very active and robust toward a large number of substrates. These precatalysts however showed activity at room temperature in alkene metathesis reactions [2,8,9]. Although they perform excellent at room temperature, they have a relatively short catalytic lifetime.



The first ^{31}P NMR investigation of a hemilabile property of S-O ligands in Pd complexes of the type $\text{trans}[\text{Pd}(\text{OOC}-\text{C}_6\text{H}_4-2\text{SR}-k^1-\text{O})\text{Ph}(\text{PPh}_3)_2]$ ($\text{R} = \text{}^i\text{Pr}, \text{}^t\text{Bu}$), wherein one PPh_3 ligand is replaced by a sulfur atom of the S-O ligand to afford chelates, in solution, was reported by Raubenheimer et al. [10]. Grubbs-type precatalysts with hemilabile ligands showed greater lifetimes and stability [10,11]. It was

also reported [12] that the electronic and steric effects, together with the ring size and rigidity of the hemilabile bidentate ligands, can possibly influence the stability of the complex to which the bidentate ligand is attached and consequently the catalytic performance. Different groups followed different design concepts of initiators in the various precatalysts to obtain thermally-switchable initiators (Scheme 1) [13].



Scheme 1. Design concepts for thermally-switchable initiators.

In the design concepts shown in Scheme 1, the intention in all is to slow down or prevent the dissociation of L². Motif A is the classical Grubbs precatalysts where L² is mostly either PCy₃ [4] or H₂IMes [7], while in Motif D, a hetero-atom like sulfur [14] is typically introduced in the alkylidene ligand of these precatalysts. Hoveyda et al. [15–18] synthesized precatalysts with Motif B that showed exceptional stability that allowed its use in reagent-grade solvents and/or in air [15], while this motif was also used by Van der Schaaf et al. [14] for the fine-tuning of gel times for the better handling of ROMP (ring-opening metathesis polymerization) in technical processes. In Motif C, where X is oxygen, the chelating ligand competes in both initiation and coordination with the incoming alkene substrate for a vacant coordination site [17]. The synthesis of this design concept was first achieved by Grubbs et al. [19] and later by Verpoort et al. [20,21]. Herrmann and co-workers synthesized the hemilabile pyridinyl alcoholato ligand-containing complexes and found low catalytic activity for ROMP; however, the activity increased with an increase in temperature as was observed for **3** [11]. A closely-related precatalyst was also synthesized by Hafner et al. [22]. Because of the increase in the catalytic lifetime as a result of hemilability, we were interested in the design concept shown in Motif C. In line with this, Jordaan [23] synthesized **4** and other ruthenium-based precatalysts by modifying the bidentate hemilabile ligand of Herrmann et al. [11] and Hafner et al. [22]. The precatalyst **4** has shown an enhanced catalyst lifetime compared to Grubbs precatalysts at 60 °C [24]. Furthermore, its optimum temperature is 80 °C in 1-octene metathesis.

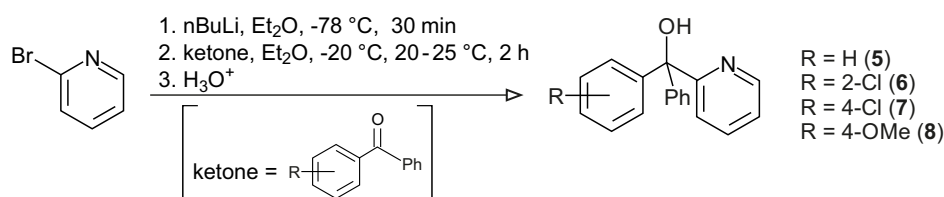
Our aim is synthesizing a precatalyst that is active, highly selective and having a longer catalytic lifetime at higher temperatures. This is because in industry, mainly linear alkenes are produced typically at high temperatures (e.g., alkenes are produced in high temperature Fischer–Tropsch processes operating at typically >300 °C [25]), thus reducing the need to lower process temperatures too low to add further value to the alkene pool. In this paper, we investigated the influence of an electron-withdrawing (Cl) and an electron-donating (OMe) substituent, *ortho* or *para* on one of the α -phenyl rings of **4**, on its catalytic performance in 1-octene metathesis. With this aim, the synthesis and characterization of *p*-chloro-, *p*-methoxy- and *o*-chloro-substituted pyridinyl alcohols and the corresponding derivatives of **4** were successfully performed. Investigations of their catalytic activity, selectivity and stability in 1-octene metathesis were made in the temperature range of 70–110 °C.

2. Results and Discussion

2.1. Synthesis of Pyridinyl Alcohols

Although there are more than 21 different methods [26] of synthesizing pyridinyl alcohols, we followed the straightforward and relatively simple synthetic route of Herrmann et al. [27] to synthesize the pyridinyl-alcohols **5–8** (Scheme 2). As was mentioned earlier, our aim is synthesizing

1-(2'-pyridinyl)-1,1-diphenyl-methanols having chlorine and/or methoxy substituents on one of the phenyl rings.



Scheme 2. Synthesis of pyridinyl alcohols 5–8.

The synthesis of the alcohols was performed in a dry and inert three-neck round-bottomed flask by stirring the mixture of nBuLi solution with 2-bromopyridine, in diethyl ether under cryogenic (−78 °C) conditions. The lithium salts of pyridinyls were then allowed to react with benzophenone, 2-chlorobenzophenone, 4-chlorobenzophenone or 4-methoxybenzophenone after raising the temperature to −20 °C for 2 h, which, in the end, was raised to room temperature, followed by careful hydrolysis. This resulted in 48% 1,1-diphenyl-1-(2'-pyridinyl)-methanol (5), 89% 1-(2'-chlorophenyl)-1-phenyl-1-(2'-pyridinyl)-methanol (6), 80% 1-(4'-chlorophenyl)-1-phenyl-1-(2'-pyridinyl)-methanol (7) and 70% 1-(4'-methoxyphenyl)-1-phenyl-1-(2'-pyridinyl)-methanol (8). The structures of the alcohols were elucidated using IR (Infrared spectrometry), NMR (Nuclear Magnetic Resonance spectrometry) and MS (Mass Spectrometry) (see Section 3). Compared to Sperber et al.'s [28] yield (14.5%), our yield for 5 is far better. They reacted picolinic acid and benzophenone (1:6) in *p*-cymene solvent for about 6 h. McCarty et al. [29] increased the yield of 5 to 25% by adding the picolinic acid over a 1–3 h period to a refluxing *p*-cymene solution of benzophenone. Using the same procedure, McCarty et al. [29] synthesized 25% of 7, which is three times less than our yield. They, however, obtained 7 (68%) and 6 (42%) by first preparing the nBuLi followed by reacting it with 2-bromopyridine at −60–−40 °C. The lithium salt of 2-bromopyridine was then reacted with 4-chlorobenzophenone and 2-chlorobenzophenone at −60 °C and then allowed to react for 2 h at −40 °C. Pyridinyl alcohol 8 was synthesized for the first time.

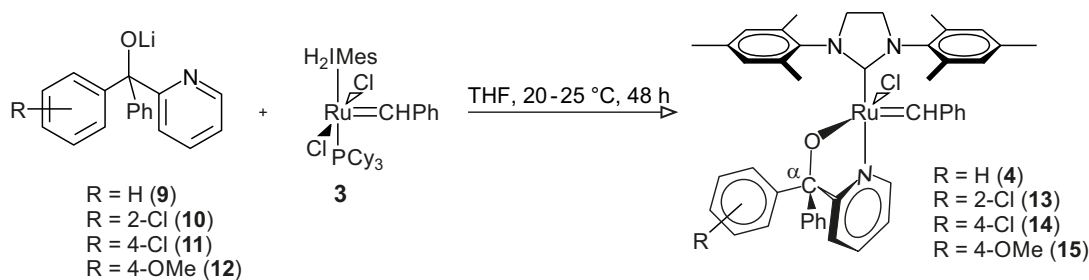
2.2. Synthesis of the Lithium Salts and the Corresponding Complexes

The lithium salts of the alcohols 5–8 were prepared in a Schlenk tube by stirring the pyridinyl alcohols with nBuLi solution in THF at room temperature in an argon atmosphere (Scheme 3) [22]. The yield percentage of the lithium salts of the pyridinyl-alcohols was not calculated, as the lithium salts are very sensitive to moisture and oxygen (air). The lithium salts were kept in the Schlenk tube under the argon atmosphere for the synthesis of the complexes shown in Scheme 4.



Scheme 3. Synthetic representation of the synthesis of the lithium salts of pyridinyl alcohols.

The lithium salts of the pyridinyl methanols 9–12 were added into a Schlenk tube containing a THF solution of the Grubbs 2 precatalyst in an argon atmosphere and stirred to result in the Grubbs 2-type precatalysts 4 and 13–15, as shown in Scheme 4.



Scheme 4. Synthetic representation of the synthesis of the ruthenium-based precatalysts.

The nitrogen chelation of the pyridinyl-alcoholato ligands to the ruthenium metal can be seen from the downfield H-6' ^1H NMR chemical shifts of the catalysts compared to the corresponding free ligands (Table 1). It is also seen from the up-field ^1H NMR chemical shift of the precatalyst carbene proton (α -H) compared to that of Grubbs 2-precatalyst. The electron donation of the pyridinyl alcoholato nitrogen to the ruthenium metal, during chelation, would possibly increase the electron density around the ruthenium and also the benzyldiene proton. This will shift its resonance up-field compared to the Grubbs 2-precatalyst. Simultaneously, the electron density on the pyridinyl-alcoholato ligand nitrogen will decrease, and this would result in the downfield chemical shift of the H-6' of pyridine. A downfield chemical shift of a proton is indicative of the decrease on the electron density around the atom [30]. Therefore, the chelation of the pyridinyl-alcoholato ligands to the ruthenium metal is evident. The precatalysts 13–15 were all synthesized for the first time, as we did not find any reported in the literature.

Table 1. Selected ^1H NMR (Nuclear Magnetic Resonance) chemical shifts of the synthesized precatalysts, Grubbs 2 and pyridinyl alcohols.

Precatalyst	$\delta_{\alpha\text{-H}}$ (ppm) ¹	$\delta_{\text{H-6}'}$ (ppm) ²	$\delta_{\text{H-6}'}$ (ppm) ³
3	19.19 ⁴	-	-
4	17.10	9.61	8.59
13	17.34/17.26	9.76	8.55
14	17.11/17.09	9.70–9.55	8.59
15	17.10/17.08	9.63–9.60	8.65

¹ ^1H NMR chemical shift of the precatalyst carbene proton (Ru = CH); ² ^1H NMR chemical shift of the pyridinyl methanolato ligand ($\text{C}_5\text{H}_3\text{N}$) H-6'; ³ ^1H NMR chemical shift of the pyridinyl methanol ($\text{C}_5\text{H}_3\text{N}$) H-6'; ⁴ obtained from [23].

The appearance of two peaks in the ^1H NMR spectra of the precatalysts 13–15 is due to the chirality of the pyridinyl alcoholato ligand at the α -position, which results in the formation of diastereomers. A similar phenomenon is observed in the ^{13}C NMR spectra.

2.3. Metathesis Reactions

The metathesis of 1-octene results in a mixture of products. The self-metathesis of 1-octene results in the formation of 7-tetradecene (*cis* and *trans*) and ethene, named primary metathesis products (PMPs). The double bond in 1-octene also undergoes isomerization to form internal olefins. The isomerization products (IPs) undergo self-metathesis and cross-metathesis reactions or secondary metathesis reactions yielding the various alkenes in the range C_3 – C_{16} named secondary metathesis products (SMPs). Table 2 summarizes the various metathesis reactions and the products of 1-octene in the presence of ruthenium alkylidene catalysts.

Table 2. Summary of products of 1-octene metathesis in the presence of ruthenium alkylidene precatalysts. PMPs (primary metathesis products); IPs (isomerization products); SMPs (secondary metathesis products).

Reaction	Substrate ¹	Products ¹	Abbreviation
Primary metathesis	-	-	-
Self-metathesis	C=C ₇	C=C + C ₇ =C ₇	PMPs
Isomerization	C=C ₇	C ₂ =C ₆ + C ₃ =C ₅ + C ₄ =C ₄	IPs
Secondary metathesis ²	-	-	-
Self-metathesis	C ₂ =C ₆	C ₂ =C ₂ + C ₆ =C ₆	SMPs
Cross-metathesis	C=C ₇ + C ₂ =C ₆	C ₂ =C ₇ + C=C ₆ + C=C ₂ + C ₆ =C ₇	

¹ Hydrogens are omitted for simplicity; ² only representative examples of SMPs are shown.

2.3.1. Effect of Temperature on Catalyst Activity and Selectivity in 1-Octene Metathesis

The effect of temperature on the catalytic activities of precatalysts **13**–**15** was investigated for temperatures of 70, 80, 90, 100 and 110 °C. The results of the metathesis reaction of 1-octene with **13** and **14** at 70 °C are not included in the figures (Figures 1 and 2) as a result of using different time intervals for sample collection than those of 80–110 °C. A summary of the results, however, is included in Tables 3 and 4. The metathesis of 1-octene was also performed using precatalyst **4** at its optimum temperature (80 °C) with the intention to compare it with the newly-synthesized precatalysts and to see the influence of the substituents on the catalytic activity. A comparison of the catalytic activity and selectivity of precatalysts **13**–**15** is also made with precatalysts **2**–**4** at their optimum temperatures. Furthermore stabilities of the precatalysts were compared in the temperature ranges 70–110 °C. The results of the metathesis reactions are presented below.

Table 3. Summary of the catalytic activity of precatalyst **13** for the metathesis of 1-octene after 540 min.

Temp. (°C)	Conv. ¹ (%)	1-Octene ²	PMPs ²	IPs ²	SMPs ²	S ³	K _{In} ⁴	TON ⁵	TOF ⁶
70	25	75	22.7	0.3	2.0	90.8	4.35 × 10 ⁻³	2039	6.3 × 10 ⁻²
80	46	54	44.2	0.1	1.9	95.7	7.40 × 10 ⁻³	3982	12.3 × 10 ⁻²
90	94	6	71.7	1.3	20.7	76.6	14.84 × 10 ⁻³	6456	19.9 × 10 ⁻²
100	95	5	69.4	1.5	24.4	72.8	9.48 × 10 ⁻³	6242	19.3 × 10 ⁻²
110	97	3	64.7	1.9	30.2	66.8	12.86 × 10 ⁻³	5824	18.0 × 10 ⁻²

¹ Conversion; ² yield in mol % and Ru/1-octene molar ratio 1:9000; ³ selectivity in percent toward PMPs;

⁴ initiation constant in mol/s; ⁵ turnover number (TON) = (n%PMPs × [nOct]/[nRu])/100 (Oct = 1-octene);

⁶ turnover frequency (TOF) = TON/s.

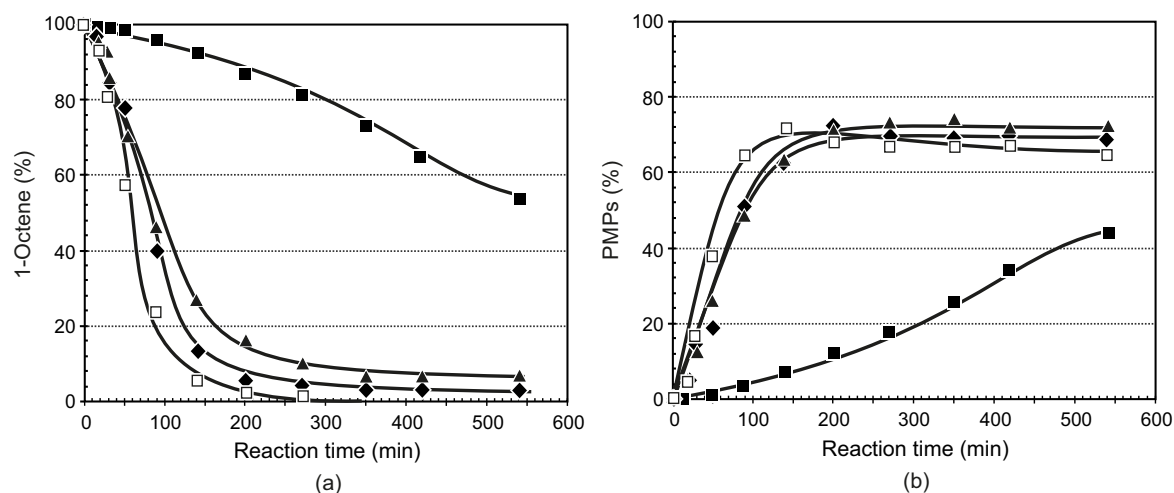


Figure 1. Cont.

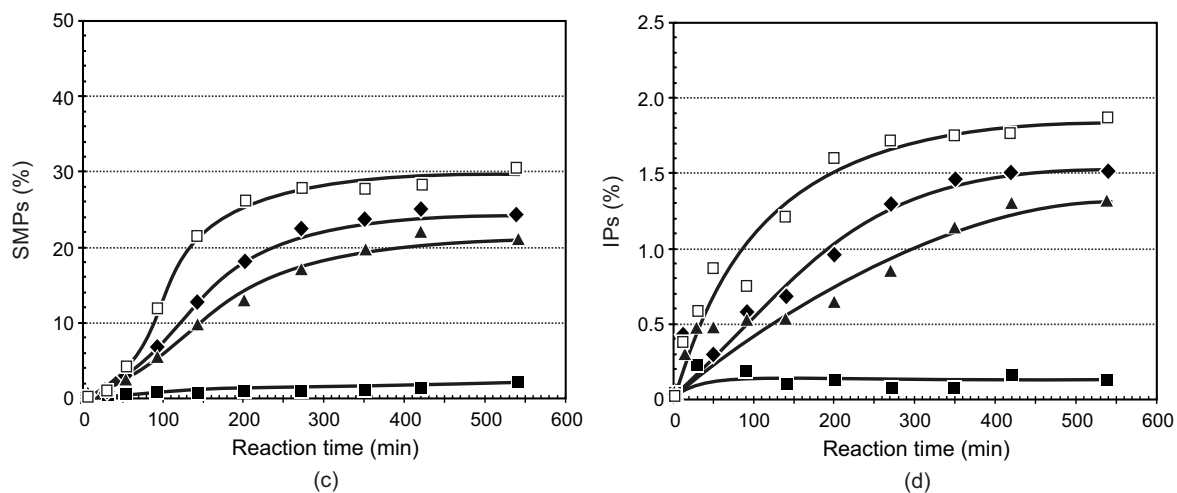


Figure 1. The influence of temperature on the reaction composition during metathesis of 1-octene using the ruthenium alkylidene precatalyst **13**: (a) conversion of 1-octene; (b) formation of PMPs (primary metathesis products); (c) formation of SMPs (secondary metathesis products); (d) formation of IPs (isomerization products); Ru/1-octene (1:9000) (■, 80 °C; ▲, 90 °C; ◆, 100 °C; □, 110 °C).

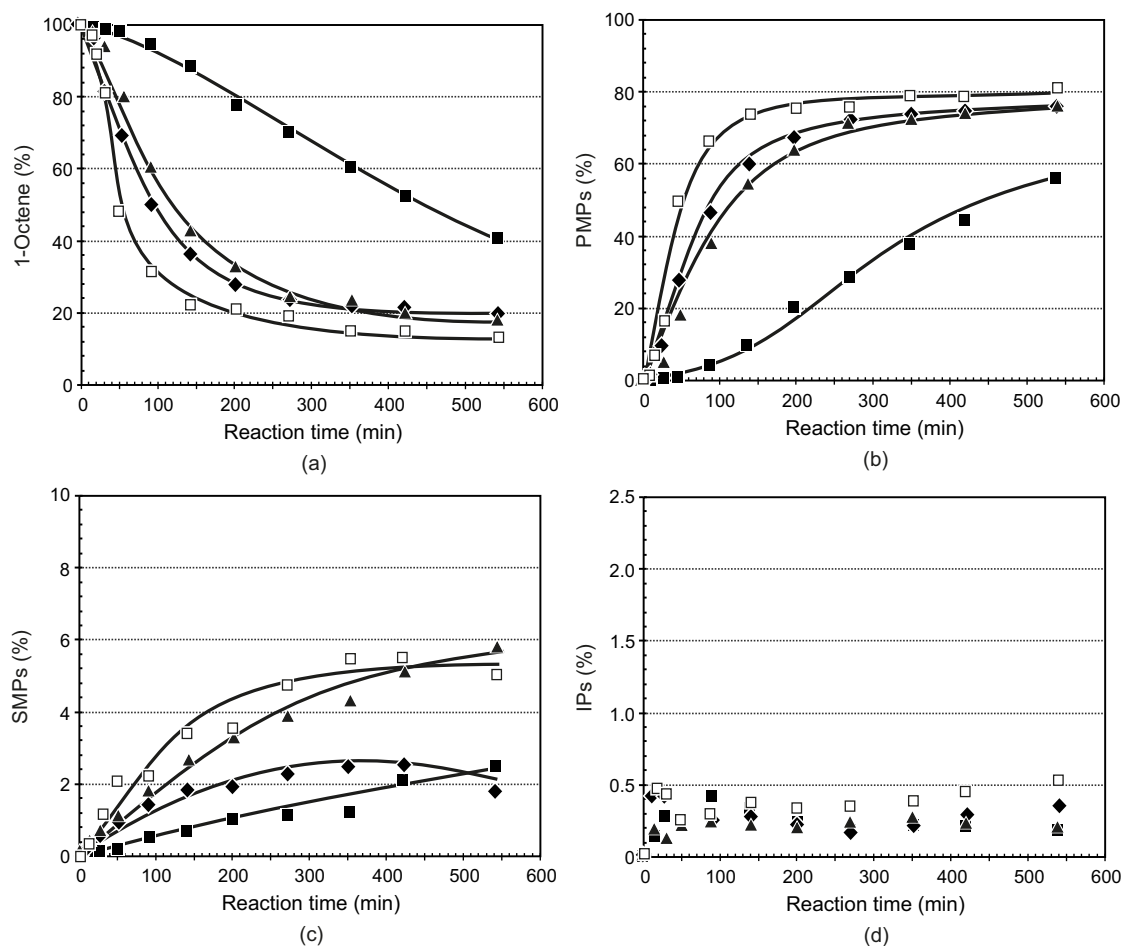


Figure 2. The influence of temperature on the reaction composition during metathesis of 1-octene using the ruthenium alkylidene precatalyst **14**: (a) conversion of 1-octene; (b) formation of PMPs; (c) formation of SMPs; (d) formation of IPs; Ru/1-octene (1:9000) (■, 80 °C; ▲, 90 °C; ◆, 100 °C; □, 110 °C).

Table 4. Summary of the catalytic activity of precatalyst **14** for the metathesis of 1-octene after 540 min.

Temp (°C)	Conv. ¹ (%)	1-Octene ²	PMPs ²	IPs ²	SMPs ²	S ³	K _{In} ⁴	TON ⁵	TOF ⁶
70	6	94	5.3	0.1	0.8	86	0.71×10^{-3}	476	1.57×10^{-2}
80	59	41	56.6	0.2	2.4	96	9.22×10^{-3}	5097	15.7×10^{-2}
90	82	18	75.8	0.2	5.8	93	11.36×10^{-3}	6823	21.1×10^{-2}
100	79	21	77.0	0.4	2.0	97	14.11×10^{-3}	6928	21.4×10^{-2}
110	87	13	81.1	0.5	5.0	94	12.75×10^{-3}	7298	22.5×10^{-2}

¹ Conversion; ² yield in mol % and Ru/1-octene molar ratio 1:9000; ³ selectivity in percent toward PMPs;

⁴ initiation constant in mol/s; ⁵ TON = ($n\%$ PMPs \times [n Oct]/[n Ru])/100; ⁶ TOF = TON/s.

Precatalyst **13** showed a progressive activity in 1-octene metathesis in the temperature range of 70–110 °C (Table 3 and Figure 1). The activity of **13**, however, is very slow at 70 °C, resulting only in 25% conversion of 1-octene to 22.7% PMPs, 2.0% SMPs and 0.3% IPs in 540 min. Although the selectivity is good (91%), the initiation constant (K_{In}), turnover number (TON) and turnover frequency (TOF) are low. The activity, however, was almost doubled on increasing the reaction temperature to 80 °C, resulting in 46% conversion of 1-octene to 44.2% PMPs, 1.9% SMPs and 1.1% IPs. The selectivity also increased to 96%, resulting in a significant increase in K_{In}, TON and TOF.

Relatively large conversion (94%) of the 1-octene into the various products was observed at 90 °C. This, however, resulted in an enormous increase in the SMPs (20.7%) and PMPs (71.7%). The IPs (1.26%) showed a very small increase as a result of the fast conversion to SMPs. A decrease in the selectivity (77%) and a large increase in the initiation constant, TON and TOF are observed due to high conversion of 1-octene to PMPs and SMPs. The increase in substrate conversion at 100 and 110 °C is not significant and led to a slight increase in SMPs (24.4% and 30.2%, respectively) and IPs (1.5% and 1.9%, respectively).

A decrease in the selectivity, K_{In}, TON and TOF was observed due to the slow 1-octene conversion. As a result of a very low activity at 70 °C, the reaction reached equilibrium, i.e., when no further PMP formation is observed, at 3630 min, wherein 85% 1-octene conversion to 80% PMPs, 4.9% SMPs and 0.2% IPs with 94% selectivity, 7214 TON and 3.3×10^{-2} TOF were observed. On the other hand, at 80 °C, equilibrium was attained at 2100 min and 79% 1-octene conversion resulting in 69% PMPs, 9.4% SMPs, and 0.2% IPs with 88% selectivity, 6237 TON and 4.94×10^{-2} TOF. At 90 °C, the reaction attained equilibrium at 350 min and 94% 1-octene conversion into 73.4% PMPs, 19.4% SMPs and 1.1% IPs with 78% selectivity, 6606 TON and 31.5×10^{-2} TOF. Although equilibrium was attained at 140 min at 100 and 110 °C, the 1-octene conversion and product distribution showed significant variation. At 100 °C, 86% conversion of 1-octene into 73% PMPs, 12.3% SMPs and 0.7% IPs was observed with 84% selectivity, 6523 TON and 77.7×10^{-2} TOF. In the case of 110 °C, 94% of 1-octene was converted into 72% PMPs, 21% SMPs and 1.2% IPs with 76% selectivity, 6456 TON and 76.9×10^{-2} TOF. Although the highest selectivity and large PMP formation and TON with relatively low SMP and IP formation are observed at 70 °C, it took a very long time to reach equilibrium. Considering the rate of the reaction, high PMPs, low SMPs and IPs, the optimum temperature for the precatalyst **13** is 80 °C.

The catalytic activity of precatalyst **14** is summarized in Table 4 and Figure 2. A very low conversion of 1-octene (6%) to PMPs (5.3%), SMPs (0.8%) and IPs (0.1%) with 86% selectivity, 476 TON, 0.71×10^{-3} K_{In} and 1.47×10^{-2} TOF is observed for 1-octene metathesis. The reaction did not even reach equilibrium after 3570 min, at which point, the reaction was stopped.

After 3570 min at 70 °C, 66% of the 1-octene was converted to 65% PMPs, 0.8% SMPs and 0.2% IPs with 99% selectivity, 5854 TON and 2.60×10^{-2} TOF. Although the 1-octene conversion, PMP formation, selectivity and TON increased significantly, the rate of the reaction is very slow. The selectivity (99%) towards PMP formation, however, is excellent at this temperature. This therefore shows the need for increasing the reaction temperature in order to increase the activity of the precatalyst and increase the rate of product formation. The reaction temperature was raised to 80 °C and resulted in 59% 1-octene conversion to 56.6% PMPs, 5.8% SMPs and 0.2% IPs with 96% selectivity, relatively high K_{In} (9.22×10^{-3}), TON (5097) and TOF (15.7×10^{-2}) after 540 min (Table 4). The 1-octene conversion

and PMP formation increased ten-fold, while the SMPs and IPs increased only two-fold in 540 min. A very large increase in selectivity, initiation constant, TON and TOF is also observed. The reaction reached equilibrium after 1620 min with 84% 1-octene conversion to 81.2% PMPs, 2.3% SMPs and 0.28% IPs with 97% selectivity, 7307 TON and 7.5×10^{-2} TOF. Further increasing the temperature to 90 °C resulted in 82% 1-octene conversion to 75.8% PMPs, 5.8% SMPs and 0.2% IPs with 93% selectivity, 6823 TON, 11.36×10^{-3} K_{In} and 21.1×10^{-2} TOF. Although all of the factors (except selectivity) showed an increase upon raising the temperature to 90 °C, further raising the temperature to 100 °C only increased the PMPs (77%), selectivity (97%), TON (6928), K_{In} (14.11×10^{-3}) and TOF (21.4×10^{-2}). The 1-octene conversion (79%), SMPs (2.0%) and IPs (0.4%), however, decreased moderately. The reaction attained equilibrium at 660 min (Figure 2) with 84% 1-octene conversion to 78.5% PMPs, 5.5% SMPs, 0.2% IPs, 93% selectivity, 7068 TON and 17.9×10^{-2} TOF at 90 °C. It required only 420 min to reach equilibrium at 100 °C (Figure 2) with 79% 1-octene conversion to 75.8% PMPs, 2.5% SMPs, 0.3 IPs and 97% selectivity, 6825 TON and 27.08×10^{-2} TOF. At 110 °C, however, 87% of the 1-octene was converted to 81.1% PMPs, 5.0% SMPs, 0.5% IP with 94% selectivity, 7298 TON, 12.75×10^{-3} K_{In} and 22.5×10^{-2} TOF at 540 min. The 1-octene conversion, PMP and SMP formation and TON showed a significant increase compared to that at 100 °C. Although the reaction seems to equilibrate at 200 min at 110 °C, the reaction slowly continued showing an increase in the substrate conversion, PMP, SMP and IP formation up to 540 min (Figure 2). Considering all of the factors, therefore, the optimum temperature for 1-octene metathesis using precatalyst 14 is 100 °C.

Figure 3 and Table 5 summarize the influence of temperature on the 1-octene metathesis reaction using precatalyst 15 after 540 min. As was the case with precatalysts 13 and 14, the 1-octene metathesis reaction using precatalyst 15 showed relatively low substrate conversion, PMP, IP and SMP formation and K_{In} , TON and TOF after 540 min. Generally, it showed low activity.

Table 5. Summary of the catalytic activity of precatalyst 15 for the metathesis of 1-octene after 540 min.

Temp (°C)	Conv. ¹ (%)	1-Octene ²	PMPs ²	IPs ²	SMPs ²	S ³	K_{In} ⁴	TON ⁵	TOF ⁶
70	17	83	15.4	0.2	1.3	91	1.82×10^{-3}	1387	4.3×10^{-2}
80	32	68	30.7	0.2	1.4	95	4.46×10^{-3}	2765	8.5×10^{-2}
90	56	44	53.4	0.2	2.1	96	7.74×10^{-3}	4802	14.8×10^{-2}
100	75	25	71.9	0.3	2.5	96	12.83×10^{-3}	6469	20.0×10^{-2}
110	97	3	91.8	0.3	4.5	95	19.01×10^{-3}	8264	25.5×10^{-2}

¹ Conversion; ² yield in mol % and Ru/1-octene molar ratio 1:9000; ³ selectivity in percent toward PMPs;

⁴ initiation constant in mol/s; ⁵ TON = ($n\%$ PMPs \times $[n\text{Oct}]/[n\text{Ru}]$)/100; ⁶ TOF = TON/s.

At 70 °C, the reaction did not reach equilibrium after 2100 min, resulting in 47% 1-octene conversion to 45% PMPs, 1.7% SMPs, 0.2% IPs and 96% selectivity, 4032 TON, 3.29×10^{-2} TOF. Increasing the temperature to 80 °C raised the 1-octene conversion to 32%, resulting in 53.4% PMPs, 1.4% SMPs, 0.2% IP and 95% selectivity, 2765 TON, 4.46×10^{-3} K_{In} and 8.5×10^{-2} TOF after 540 min. The substrate conversion and PMP formation, K_{In} , TON and TOF are doubled, while the SMP formation showed a moderate increase, and IP formation decreased. The reaction did not equilibrate after 2100 min, resulting in 84% 1-octene conversion to 81% PMPs, 2.9% SMPs, 0.1% IPs, 97% selectivity, 7321 TON and 5.8×10^{-2} TOF. Raising the temperature to 90 °C converted 56% of 1-octene to 53.4% PMPs, 2.1% SMPs, 0.2% IPs and 96% selectivity, 4802 TON, 7.74×10^{-3} K_{In} and 14.8×10^{-2} TOF after 450 min. Except for IP formation and selectivity, a substantial increase was observed in all of the factors upon increasing the temperature by 10 °C.

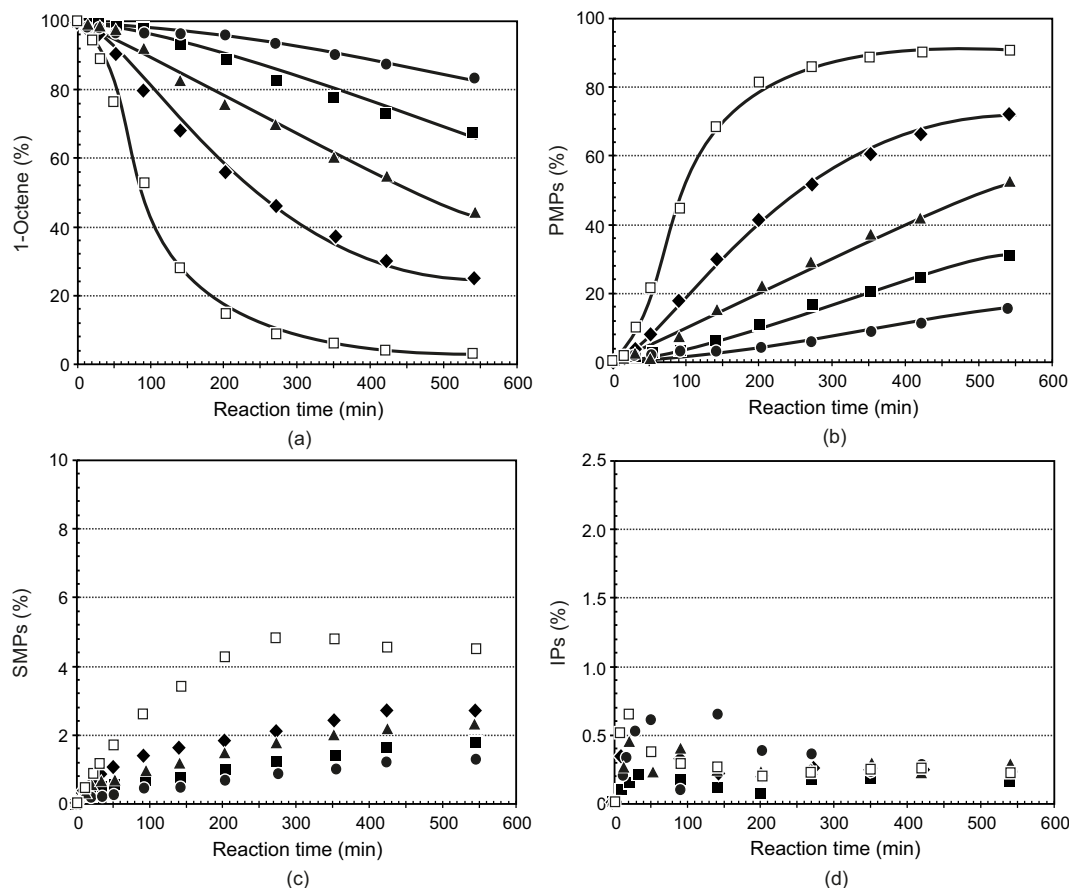


Figure 3. The influence of temperature on the reaction composition during metathesis of 1-octene using the ruthenium alkylidene pre-catalyst 15: (a) conversion of 1-octene; (b) formation of PMPs; (c) formation of SMPs; (d) formation of IPs; Ru/1-octene (1:9000) (●, 70 °C; ■, 80 °C; ▲, 90 °C; ◆, 100 °C; □, 110 °C).

The reaction, however, did not reach equilibrium at 2100 min, where it was stopped, resulting in 91% conversion of 1-octene to 87% PMPs, 4.1% SMPs, 0.2% IPs, 95% selectivity, 7835 TON and 6.2×10^{-2} TOF. Relatively high substrate conversion to high PMPs and SMPs is observed after 2100 min. At 100 °C, 75% of the 1-octene was converted to 71.9% PMPs, 2.5% SMPs and 0.3% IPs with 96% selectivity, 6469 TON, 12.83×10^{-3} K_{In} and 20.0×10^{-2} TOF after 540 min. The increase in 1-octene conversion to PMPs is significant, while its conversion to SMPs and IPs is relatively small. The TON, K_{In} and TOF also showed a substantial increase. The reaction, however, reached equilibrium after 780 min with 84% of substrate conversion to 81% PMPs, 3.5% SMPs, 0.3% IPs, 96% selectivity, 7251 TON and 15.5×10^{-2} TOF. In spite of all of the variations in substrate conversion, PMP, SMP and IP formation, the selectivity remained the same (96%), which is a remarkable phenomenon. As a result of the relatively small SMP and IP formation, we were interested to see the influence of the reaction temperature at 110 °C on the catalytic performance of 15. As is shown in Table 5 and Figure 3, 97% of the 1-octene was converted to 91.8% PMPs, 4.5% SMPs, 0.3% IPs with 95% selectivity, 8264 TON, 19.01×10^{-3} K_{In} and 26.0×10^{-2} TOF after 540 min. This is a remarkable result, which we did not see with any of the previous pre-catalysts at this temperature after 540 min. In addition to this, the reaction attained equilibrium after 660 min with 97% of the substrate being converted to 93% PMPs, 4.3% SMPs, 0.2% IPs with 95% selectivity, 8340 TON and 21.1×10^{-2} TOF. It is exciting to see nearly all of the 1-octene being converted to PMPs. It is difficult to decide the optimum reaction temperature for pre-catalyst 15 as a result of similar selectivities towards PMPs at the high temperatures. Therefore, we prefer to consider both 100 and 110 °C as optimum temperatures for pre-catalyst 15.

2.3.2. Comparison of Catalytic Activity and Selectivity

Table 6 and Figure 4 show a summary and comparison respectively of the catalytic activities of precatalysts 2–4 and 13–15 in 1-octene metathesis at 80 °C after 540 min. We choose 80 °C because the optimum temperature for precatalyst 4, our reference precatalyst, is 80 °C, as it will help us compare the influence of the substituents on the catalytic activities of precatalysts 13–15. We also included the first and second generation Grubbs precatalysts 2 and 3 for the sake of comparing the improvement in terms of the catalyst activity at high temperatures. As we have mentioned earlier, our main objective is to synthesize a catalyst that would perform better at high temperatures so that it could be considered for industrial applications.

Table 6. Summary of the catalytic activity of different precatalysts for the metathesis of 1-octene at 540 min and 80 °C.

Catalyst	Conv. ¹ (%)	1-octene ²	PMPs ²	IPs ²	SMPs ²	S ³	K _{in} ⁴	TON ⁵	TOF ⁶
2	83.2	16.8	58.0	25.2	0.5	69	9.36×10^{-3}	5179	16.0×10^{-2}
3	96	4.0	67.0	3.0	26.0	70	7.91×10^{-3}	6029	18.6×10^{-2}
4	77	23.2	74.0	2.7	0.2	96	10.66×10^{-3}	6643	20.5×10^{-2}
13	46	53.7	44.0	1.9	0.1	96	7.40×10^{-3}	3982	12.3×10^{-2}
14	59	40.8	57.0	2.3	0.2	96	9.22×10^{-3}	5097	15.7×10^{-2}
15	32	68.0	31.0	1.4	0.2	95	4.46×10^{-3}	2765	8.5×10^{-2}

¹ Conversion; ² yield in mol % and Ru/1-octene molar ratio 1:9000; ³ selectivity in percent toward PMPs;

⁴ initiation constant in mol/s; ⁵ TON = ($n\%$ PMPs \times [nOct]/[nRu])/100; ⁶ TOF = TON/s.

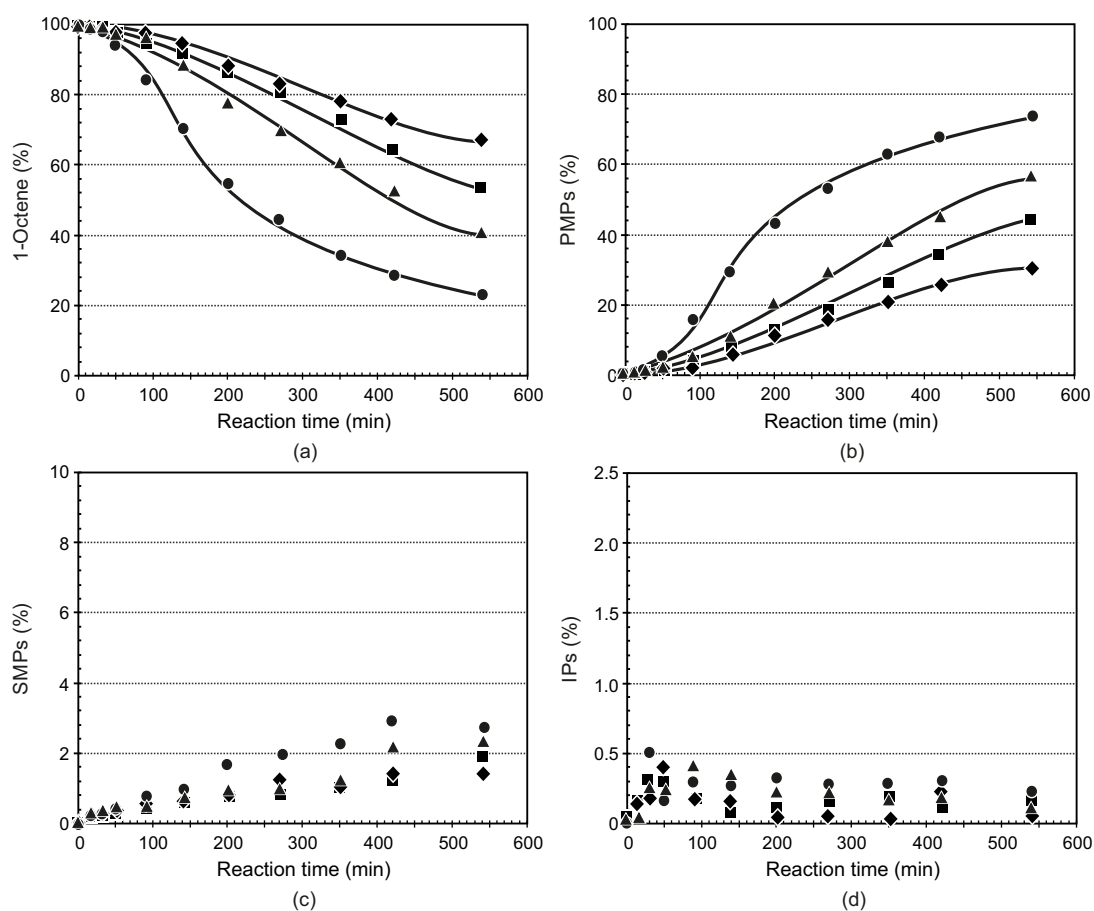


Figure 4. Comparison of catalytic activity, selectivity and stability of precatalysts 4 and 13–15 during the course of metathesis of 1-octene: (a) conversion of 1-octene; (b) formation of PMPs; (c) formation of SMPs; (d) formation of IPs; Ru/1-octene (1:9000), 80 °C (●, 4; ■, 13; ▲, 14; ◆, 15).

Although high 1-octene conversion is observed for precatalysts **2** and **3**, the highest PMP formation, selectivity, K_{In} , TON and TOF is observed for precatalyst **4**. The lowest catalytic activity is observed for **15**. Precatalysts **14** and **13** rank second and third, respectively. The precatalyst **3** resulted in relatively high SMPs, although it showed comparative TON and TOF to precatalysts **13** and **14**. Precatalyst **2**, on the other hand, resulted in high IP (25%) formation that made the reaction competitive regarding IP and PMP formation. The competitive reaction products in **2** and **3** made the selectivity toward PMPs become relatively small.

The relatively low 1-octene conversion and PMP formation for precatalyst **15** is due to the fact that the reaction temperature is way below its optimum temperature. To this effect, we wanted to compare the catalytic performances of all of the aforementioned precatalysts at their optimum temperatures after 420 min. Jordaan [23] optimized the 1-octene metathesis reaction of **2** and **3** at a 1-octene/Ru molar ratio of 9000 and found the optimum reaction temperatures to be 35 and 60 °C, respectively. Table 7 presents the results of the catalytic activities of all of the precatalysts at their optimum temperatures for 1-octene metathesis.

Table 7. Summary of the catalytic activity of different precatalysts for the metathesis of 1-octene after 420 min and at optimum reaction temperatures.

Catalyst	Temp (°C)	1-Octene ²	PMPs ²	IPs ²	SMPs ²	S ³	K_{In} ⁴	TON ⁵	TOF ⁶
2	35 ⁷	58.5	40.8	0.4	0.3	98	0.12×10^{-4}	4136	16.4×10^{-2}
3	60 ⁷	14.8	81.6	0.0	3.6	96	1.89×10^{-4}	8881	35.2×10^{-2}
4	80	28.8	68.0	0.3	2.9	96	9.60×10^{-3}	6120	24.3×10^{-2}
13	80	65.5	34.0	0.2	1.3	96	5.32×10^{-3}	3063	12.2×10^{-2}
14	100	21.2	76.0	0.3	2.5	97	13.54×10^{-3}	6825	27.1×10^{-2}
15	100	30.2	67.0	0.3	2.5	96	11.57×10^{-3}	6005	23.8×10^{-2}
15	110	4.2	91.0	0.3	4.5	95	17.12×10^{-3}	8160	32.4×10^{-2}

¹ Conversion; ² yield in mol % and Ru/1-octene molar ratio 1:9000; ³ selectivity in percent toward PMPs; ⁴ initiation constant in mol/s; ⁵ TON = ($n\%$ PMPs \times $[n\text{Oct}]/[n\text{Ru}]$)/100; ⁶ TOF = TON/s; ⁷ data obtained from [23].

The lowest catalytic activity is observed for **13** in every aspect (except selectivity), and the highest selectivity is observed for **2**. The highest substrate conversion and PMPs formation is observed for **15** (at 110 °C), which is followed by **3**. Precatalyst **3**, however, resulted in relatively high TON and TOF followed by **15** (at 110 °C). Precatalysts **15** (at 100 °C) and **4** showed similar activities, whereas precatalyst **14** showed better activity than these two. Generally, precatalysts **14** and **15** showed better activity than the rest of the precatalysts at high temperatures (100 and 110 °C). Therefore, we improved the optimum temperature of the very stable precatalyst **4** to temperatures as high as 100 and 110 °C, sustaining high catalyst activity and selectivity by introducing chloro and methoxy groups on the *p*-position of one of the α -phenyl groups in the pyridinyl alcoholato ligand.

2.3.3. Effect of Temperature on the Catalyst Lifetime

Previously [24,31], we reported the stability (as seen in the improved catalytic lifetimes) of precatalyst **4** and other related precatalysts *inter alia* by using the plot of the \ln ([starting material]) versus time. According to Grubbs and co-workers [32], a linear plot indicates a reaction with pseudo-first order rate kinetics, while a curved plot points towards catalyst decomposition. In this article, we use the same approach in order to compare catalyst stability.

The plots of precatalysts **13** and **14** show catalytic stability at 70 and 80 °C, while the precatalyst **15** showed relatively better catalytic stability between 70 and 100 °C (Figure 5). The deviation from linearity after 470 min in the course of the metathesis reaction of precatalyst **15** reveals its high stability even at 110 °C, while precatalysts **13** and **14** started catalyst decomposition already after 270 min at 90 °C, after 200 min at 100 °C and after 140 min at 110 °C. Although precatalysts **14** and **15** perform very well at 100 °C, precatalyst **15** shows better catalyst stability, and therefore, it will be a choice of interest for high temperature industrial olefin metathesis reactions. In our previous work [24], we

reported that the Grubbs second generation precatalyst **3** resulted in a curved plot at 60 °C; therefore, all of the precatalysts **13–15** showed better catalyst stability at temperatures as high as 80 °C (**13** and **14**) and 100 °C (**15**). Comparing only with our reference precatalyst **4**, all of the substituted precatalysts showed a better lifetime as a result of a slightly curved plot at 80 °C in the case of precatalyst **4** (Figure 5d).

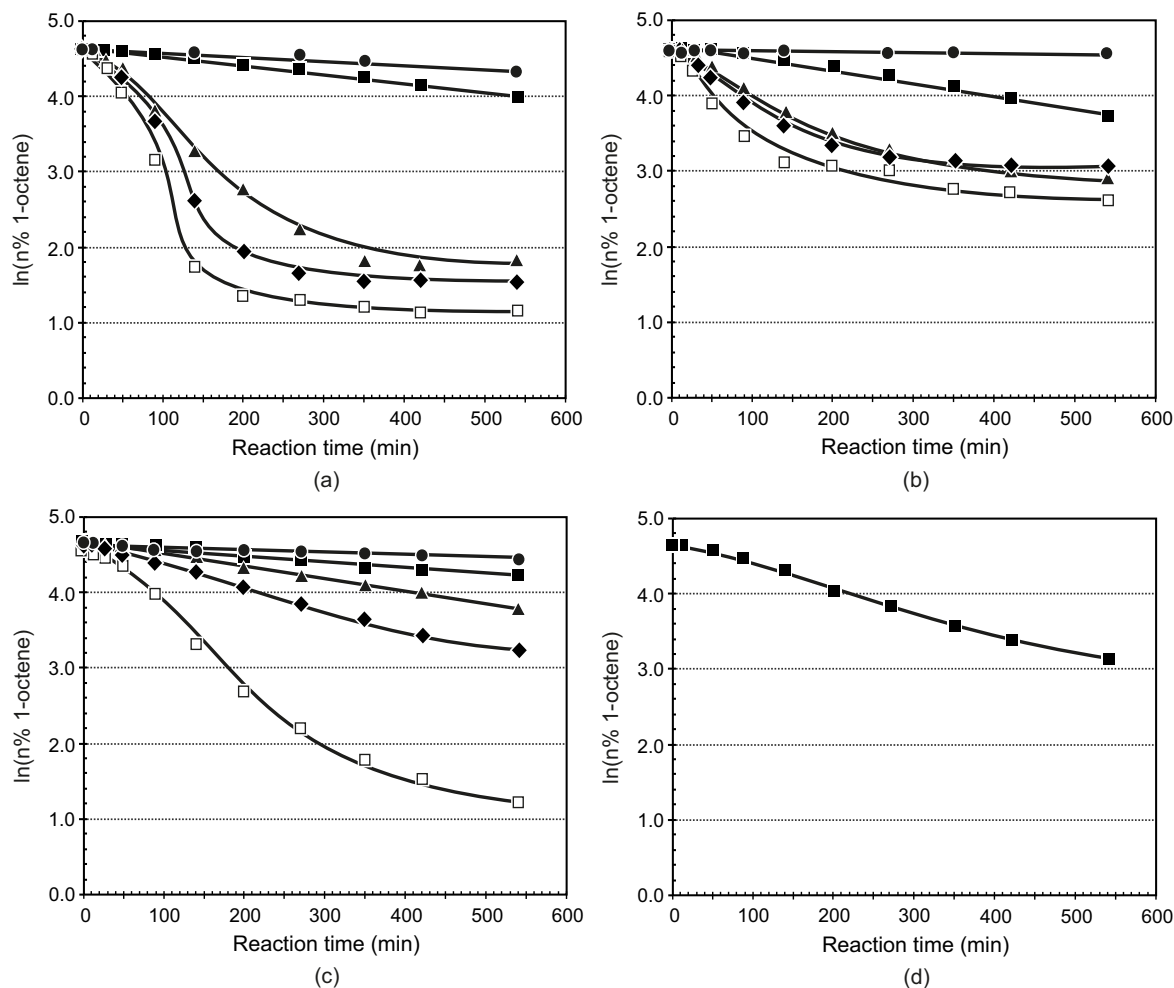


Figure 5. $\ln([n\%1\text{-octene}])$ versus time plots of: (a) precatalyst **13**; (b) precatalyst **14**; (c) precatalyst **15**; (d) precatalyst **4** (●, 70 °C; ■, 80 °C; ▲, 90 °C; ◆, 100 °C; □, 110 °C).

So far, we have been discussing the catalytic activities and stabilities of the precatalysts in 1-octene metathesis. Generally, the experimental results revealed the fact that the substituted precatalysts **13–15** are more stable than the unsubstituted precatalyst **4**. Our comparison in terms of catalytic performance showed the fact that the 4-chloro/methoxy-substituted pyridinyl alcoholato precatalysts **14** and **15** perform better than the 2-chlorosubstituted precatalyst **13** and the unsubstituted precatalyst **4** at high temperatures (≥ 80 °C). The question is, therefore, what is the reason behind this? Is it electronic, steric or the combination of the two? To answer these questions and to get a fundamental understanding of the differences in catalytic performance and catalyst stability among the precatalysts under investigation, a DFT (Density Functional Theory) study was performed.

2.4. Molecular Modelling

In the DFT study, the precatalysts **4** and **13–15** were optimized using the DMol³ module of Accelrys Material Studio 6.1 (Accelrys Software Inc., San Diego, CA, USA) [33]. Steric calculations between

atoms and/or groups was calculated using Solid Angle [34], and energy calculations were performed based on previous work [35]. Table 8 presents the calculated properties of the precatalysts where all properties were obtained from the Gaussian output files using the pop = NBOread (NBO = natural bond order) keyword.

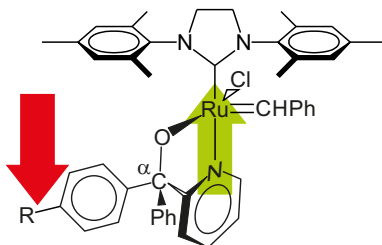


Figure 6. Visual representation of forces (red and green arrows) contributing to the higher activity and stability of catalysts with ligands on the 4-position of one of the α -phenyl groups in the pyridinyl alcoholato ligand.

Table 8. Experimental data and calculated properties of precatalyst 4 and 13–15.

Catalyst	Temp (°C)	PMPs ¹	C–C _C ^{2,3}	Ru–N _C ³	Ru (NPA) ⁴	N (NPA) ⁴	Wiberg (Ru–N)
13	80	34	0.34	2.190	0.148	−0.368	0.391
4	80	68	none	2.186	0.140	−0.361	0.402
15	100	67	0.81	2.187	0.140	−0.358	0.404
14	100	76	1.73	2.180	0.138	−0.358	0.406

¹ Yield in mol %; ² C–C_C is the close contact between the carbene carbon and NHC (N-heterocyclic carbene) carbon; ³ the subscript indicates the closed system of the precatalyst as shown in Figure 6; ⁴ NPA is the natural population analysis; the close contacts and bond lengths are measured in Å.

Table 9 summarizes the observed trends of the calculated properties based on experimental data. Most of the calculated properties fit well to the observed experimental result. The observed close contact order 13 > 15 > 14 between the carbene carbon and the sterically bulky NHC (N-heterocyclic carbene) group indicates the possibility of relatively high steric repulsion between the 4-substituted chlorine and/or methoxy groups and the NHC, which leads to the reorganization of the structure, resulting in the aforementioned close contact order.

Table 9. Summary of observed trends based on the experimental and calculated results.

Experimentally Observed	Increasing Order of Values	Trend
Optimum Temperature ^c	→	13 4 15 = 14
PMPs ^d	→	13 4 15 14
Calculated properties		
Close contact of C _{carbene} and C _{NHC}	→	4 ^a 13 15 14
N _{natural charge}	→	13 4 15 14
Wiberg bond index for Ru–N	→	13 4 15 14
Bond length Ru–N	←	13 15 4 ^b 14
Ru _{natural charge}	←	13 4 15 14

^a None observed for 4; ^b the bond length of 4 is only 0.0015 Å greater than 15; ^c considering 100 °C for precatalyst 15; ^d at optimum temperature.

The highest close contact [34] for precatalyst 14 was due to the relatively large size of the chloro group compared to the methoxy oxygen. This steric repulsion can affect the Ru–N bond length, as can be seen in Figure 6, hence the Ru–N bond length order in Table 9. The shorter the Ru–N bond length, the slower the hemilability of the pyridinyl alcoholato ligand at a low temperature. Therefore, the

relatively high optimum temperature for the precatalysts **14** and **15** is as a result of the strong Ru–N bond. It is therefore the combination of steric and electronic effects that contributed to the differences in the catalyst performance.

According to Wiberg [36], the larger the Wiberg index value, the more active the carbene double bond of the precatalyst. In other words, a π -system can be more active if there exists high electron density. Incidentally, therefore, in the precatalyst **14**, the bonding electrons are denser than the rest of the catalysts. This is therefore in agreement with the theoretically-calculated Ru–N bond length order. The only switch between Wiberg's index and Ru–N bond length order is between precatalysts **4** and **15**; otherwise, it is in good agreement with the experimental results. The Ru and N natural charges also signify the fact that the closer the nitrogen to the ruthenium, the more the electron density (less positive charge) around the ruthenium and the less the negative charge on the nitrogen; hence, the ruthenium charge order of the precatalysts is $13 > 4 > 15 > 14$.

3. Materials and Methods

3.1. Instrumental Methods

IR spectra were obtained by using a Bruker ALPHA-P FTIR (Bruker Optik GmbH, Ettlingen, Germany) equipped with an ATR (attenuated total reflection). A small amount of solid samples was applied directly onto the ATR.

$^1\text{H-NMR}$ (CDCl_3 , 600 MHz), $^{13}\text{C-NMR}$ (150 MHz), $^{31}\text{P-NMR}$ (CDCl_3 , 242 MHz), DEPT135 (CDCl_3 , 150 MHz), COSY (CDCl_3 , 600 MHz) and HSQC (CDCl_3 , 600 MHz and 150 MHz) spectra were obtained using a Bruker Ultrashield Plus 600 Avance III spectrometer (Bruker BioSpin GmbH, Rheinstetten, Germany). Samples were prepared by dissolving 20 mg of the sample in 0.75 mL CDCl_3 .

The masses of the alcohols and the complexes were determined using time-of-flight mass spectrometry (TOF-MS) with the following ionization techniques: atomic pressure chemical ionization (APCI), electron spray ionization (ESI) and matrix-assisted laser desorption ionization (MALDI). A Bruker MicrOTOF-Q II 10390 MS (Bruker Daltonik GmbH, Bremen, Germany) with APCI using the following parameters was used: number of scans 400–1500 m/z , positive ion polarity, capillary 4000 V, endplate offset –500 V, collision cell RF 350.0 Vpp, nebulizer 2.2 bar, dry heater 200 °C, dry gas 6.0 L/min. A Bruker MicrOTOF-Q II 10390 MS (Bruker Daltonik GmbH, Bremen, Germany) with ESI using the following parameters was used: scans between 50 and 1500 m/z , positive ion polarity, capillary 4500 V, endplate offset –500 V, collision cell RF 100.0 Vpp, nebulizer 0.4 bar, dry heater 180 °C, dry gas 4.0 L/min. A Bruker Autoflex TOF/TOF MS (Bruker Daltonik GmbH, Bremen, Germany) with MALDI using the following parameters was used: laser (laser beam attenuation 99, laser beam focus 64, laser repetition rate 250 Hz, number of shots 500), positive voltage polarity, PIE (pulsed ion extraction) delay 140 ns, ion source voltage 1 1.9 kV, ion source voltage 2 16.65 kV, lens voltage 7.8 kV, linear detector voltage 0 kV, deflection on true, deflection mass 400 Da, Reflector Voltage 1 21 kV, Reflector Voltage 2 9.55 kV, reflector detector voltage 1.775 kW. Sample preparation for MALDI-MS: 20 mg/mL in THF DCTB and 1 mg sample were dissolved in 1 mL CHCl_3 . Ratio of DCTB:sample 20 $\mu\text{L}:\mu\text{L}$; 1 μL of mixture was placed on a ground steel target plate.

Melting points of the pyridinyl alcoholato ligands and decomposition points of the precatalysts were determined with a Büchi B-540 melting point apparatus.

Gas chromatography/MS (GC/MS) analyses of the 1-octene metathesis reactions were performed on an Agilent 6890 (Agilent Technologies, Santa Clara, CA, USA) gas chromatograph equipped with an Agilent 7683B autosampler, HP-5 capillary column and an Agilent 5973 mass selective detector (MSD). The same oven program was used with either a two-minute solvent delay or no solvent delay. Helium was used as carrier gas with a 1.5-mL/min flow rate at 20 °C. The following general GC settings were used: column: HP-5, 30.0 m \times 320 μm \times 0.25 μm ; split ratio: 0.1:1; split flow: 0.1 mL/min; inlet: 250 °C, 16.6 kPa; injection volume: 0.2 μL ; detector: 50–550 Dalton mass range; scan speed of 2.94 s per

decade; oven programming: 60 °C (hold time 2 min); 60 to 110 °C at 25 °C/min; 110 °C (hold time 10 min); 110 to 290 °C at 25 °C/min (hold time 16 min).

3.2. Materials and Reagents

2-Bromopyridine (99%), nBuLi (2.5 M in hexane), benzophenone (99%), 2-chlorobenzophenone (99%), 4-chlorobenzophenone (99%), 4-methoxybenzophenone (99%), Grubbs first generation (97%) and Grubbs second-generation (97%) catalysts were purchased from Sigma Aldrich (Sigma-Aldrich® South Africa, Johannesburg, South Africa). Diethyl ether and THF were dried over Na in the presence of benzophenone, and pentane is distilled in CaH₂ in inert atmosphere before using as a solvent. A gastight Hamilton syringe (Hamilton, Bonaduz, GR, Switzerland) was used to add air-sensitive reagents and dried solvents to the reaction vessel. The Acrodisc Premium 25-mm syringe filter with GxP/0.45 µm GHP (GH Polypro) membrane (PALL Corporation, Port Washington, NY, USA) was used to filter the lithium salt from the precatalyst.

3.3. Synthesis Methods

3.3.1. General Procedure for the Synthesis of Ligands 5–8

Diethyl ether (50 mL) was added to a three-neck round-bottom flask (200 mL) in argon and cooled to −78 °C. To this, nBuLi (50 mmol, 2.5 M in hexane) was added slowly, which then was followed by the drop-wise addition of 2-bromopyridine (47.5 mmol, in 12.5 mL diethyl ether) at −78 °C, and the mixture was stirred for 15 min, resulting in a dark-red solution. The reaction temperature was raised to −20 °C, and mono ortho- and/or para-chloro and/or para-methoxy substituted benzophenone/benzophenone (52.5 mmol, in 20 mL diethyl ether) was added slowly to the reaction mixture and the mixture stirred for 2 h. The temperature was raised to room temperature, and the reaction mixture was hydrolysed carefully. The organic phase was separated from the aqueous phase and then extracted with 2 M HCl (5 × 10 mL). The aqueous phase was neutralized with a 2 M NaOH solution and extracted with diethyl ether. The organic phases were combined, dried with MgSO₄, and the solvent was slowly evaporated to obtain a white crystalline solid product.

1,1-diphenyl-1-(2'-pyridinyl)-methanol, **5**: Yield 5.96 g, 48%, white crystalline solid, m.p. (melting point): 105 °C, ¹H NMR (CDCl₃, 600 MHz, CDCl₃); δ_H = 8.59 (d, *J* = 4.9 Hz, 1H, H-6 of C₆H₄N), 7.62 (td, *J*¹ = 7.7 Hz, *J*² = 1.8 Hz, 1H, H-4 of C₆H₄N), 7.45–7.19 (m, 11H, H-5 of C₅H₄N & 10H of 2Ph), 7.12 (d, *J* = 7.9 Hz, 1H, H-3 of C₆H₄N), 6.30 (s, 1H, OH); ¹³C NMR (CDCl₃, 150 MHz): δ_C = 163.2 (qC, C-2 C₆H₄N), 147.7 (CH, C-6 C₆H₄N), 146.1 (2qC, C-1 Ph), 136.4 (CH, C-4 C₆H₄N), 128.1 (4CH, C-3 & C-5 Ph), 127.3 (4CH, C-2 & C-6 Ph), 122.9 (2CH, C-4 Ph & C-3 C₆H₄N), 122.3 (CH, C-5 C₆H₄N), 80.8 (C–OH); M⁺ (APCI, *m/z*): calculated 261.1153 (C₁₈H₁₅NO), found 262.1191 (C₁₈H₁₆NO), 261.1117 (C₁₈H₁₅NO), 260.1045 (C₁₈H₁₄NO), 244.1121 (C₁₈H₁₄N). IR (neat): ν(OH) = 3342 cm^{−1}, ν(C–H, aromatic) = 3075 cm^{−1}, 3018 cm^{−1}, 756 cm^{−1}, ν(C=C & N=C, aromatic) = 1591 cm^{−1}, 1571 cm^{−1}, ν(C–O, aliphatic) = 1168 cm^{−1}, 1126 cm^{−1}.

1-(2'-chlorophenyl)-1-phenyl-1-(2'-pyridinyl)-methanol, **6**: Yield 9.81 g, 89%, white crystalline solid, m.p.: 122 °C, ¹H NMR (CDCl₃, 600 MHz, CDCl₃); δ_H = 8.54 (d, 1H, *J* = 4.64 Hz, H-6 of C₆H₄N), 7.60 (dt, 1H, *J* = 7.73, 1.69 Hz, H-4 of C₆H₄N), 7.12 (d, 1H, *J* = 7.87 Hz, H-3 of C₆H₄N), 7.04 (t, 1H, *J* = 7.67 Hz, H-4 of substituted Ph), 6.76 (t, 1H, *J* = 7.87 Hz, H-3 of substituted Ph), 7.15–7.36 (m, 8H, H-5 of C₆H₄N and Ph); ¹³C NMR (CDCl₃, 150 MHz): δ_C = 162.5 (q C-2 C₆H₄N), 147.8 (CH, C-6 C₆H₄N), 136.5 (CH, C-4 C₆H₄N), 122.6 (CH, C-3 C₆H₄N), 122.3 (CH, C-5 C₆H₄N), 144.5 (qC, C-1 substituted Ph), 134.7 (qC, C-2 substituted Ph), 131.7 (CH, C-2 substituted Ph), 130.9 (CH, C-3 substituted Ph), 127.2 (CH, C-3 substituted Ph), 127.5 (CH, C-4 substituted Ph), 142.7 (qC, Ph), 128.0 (2CH, C-2 Ph), 129.1 (2CH, C-3 Ph), 125.9 (CH, C-4 Ph), 81.0 (qC, COH); M⁺ (APCI, *m/z*): calculated 295.0763 (C₁₈H₁₄ClNO), found 295.0757 (C₁₈H₁₄ClNO), 296.0826 (C₁₈H₁₅ClNO), 278.0739 (C₁₈H₁₃ClN); IR (neat): ν(OH) = 3347 cm^{−1},

$\nu(\text{C-H, aromatic}) = 3059 \text{ cm}^{-1}, 3005 \text{ cm}^{-1}, 753 \text{ cm}^{-1}, \nu(\text{C=C \& N=C, aromatic}) = 1590 \text{ cm}^{-1}, 1568 \text{ cm}^{-1}, \nu(\text{C-O, aliphatic}) = 1169 \text{ cm}^{-1}, 1138 \text{ cm}^{-1}.$

1-(4'-chlorophenyl),1-phenyl-1-(2'-pyridinyl)-methanol, **7**: Yield 11.23 g, 80%, white crystalline solid, m.p.: 110 °C, $^1\text{H NMR}$ (CDCl_3 , 600 MHz, CDCl_3); $\delta_{\text{H}} = 8.58$ (d, 1H, $J = 4.56$ Hz, H-6 of $\text{C}_6\text{H}_4\text{N}$), 7.64 (dt, 1H, $J = 8.02, 1.64$ Hz, H-4 of $\text{C}_6\text{H}_4\text{N}$), 7.07 (d, 1H, $J = 8.97$ Hz, H-3 of $\text{C}_6\text{H}_4\text{N}$), 7.21–7.31 (m, 10H, H-5 of $\text{C}_6\text{H}_4\text{N}$ & 2Ph), 6.27 (s, 1H, OH); $^{13}\text{C NMR}$ (CDCl_3 , 150 MHz): $\delta_{\text{C}} = 162.6$ (qC, C-2 $\text{C}_6\text{H}_4\text{N}$), 147.8 (CH, C-6 $\text{C}_6\text{H}_4\text{N}$), 136.5 (CH, C-4 $\text{C}_6\text{H}_4\text{N}$), 122.7 (CH, C-3 $\text{C}_6\text{H}_4\text{N}$), 122.5 (CH, C-5 $\text{C}_6\text{H}_4\text{N}$), 145.6 (qC, C-1 substituted Ph), 131.3 (qC, C-4 substituted Ph), 129.5 (2CH, C-2 substituted Ph), 128.0 (6CH, C-3 substituted Ph, C-2 & C-3 Ph), 144.7 (qC, C-1 of Ph), 127.5 (CH, C-4 Ph), 80.4 (qC, COH); M^+ (APCI, m/z): calculated 295.0763 ($\text{C}_{18}\text{H}_{14}\text{ClNO}$), found 295.0745 ($\text{C}_{18}\text{H}_{14}\text{ClNO}$), 296.0800 ($\text{C}_{18}\text{H}_{15}\text{ClNO}$), 294.0674 ($\text{C}_{18}\text{H}_{13}\text{ClNO}$), 278.0727 ($\text{C}_{18}\text{H}_{13}\text{ClN}$); IR (neat): $\nu(\text{OH}) = 3373 \text{ cm}^{-1}, \nu(\text{C-H, aromatic}) = 3072 \text{ cm}^{-1}, 3021 \text{ cm}^{-1}, 816 \text{ cm}^{-1}, \nu(\text{C=C \& N=C, aromatic}) = 1589 \text{ cm}^{-1}, 1570 \text{ cm}^{-1}, \nu(\text{C-O, aliphatic}) = 1169 \text{ cm}^{-1}, 1093 \text{ cm}^{-1}.$

1-(4'-methoxyphenyl),1-phenyl-1-(2'-pyridinyl)-methanol, **8**: Yield 9.5 g, 70%, white crystalline solid, m.p.: 121.6 °C, $^1\text{H NMR}$ (CDCl_3 , 600 MHz, CDCl_3); $\delta_{\text{H}} = 8.57$ (d, 1H, $J = 4.85$ Hz, 6-H of $\text{C}_6\text{H}_4\text{N}$), 7.62 (dt, 1H, $J = 7.81, 1.58$ Hz, H-4 of $\text{C}_6\text{H}_4\text{N}$), 7.08 (d, 1H, $J = 7.19$ Hz, H-3 of $\text{C}_6\text{H}_4\text{N}$), 7.17 (d, 2H, $J = 8.87$ Hz, H-2 & H-6 of substituted Ph), 6.81 (d, 2H, $J = 8.65$ Hz, H-3 & H-5 of substituted Ph), 7.19–7.28 (m, 6H, H-5 of $\text{C}_6\text{H}_4\text{N}$ & Ph), 6.21 (s, 1H, OH), 3.77 (s, 3H, OCH_3); $^{13}\text{C NMR}$ (CDCl_3 , 150 MHz): $\delta_{\text{C}} = 158.7$ (qC, C-2 $\text{C}_6\text{H}_4\text{N}$), 147.6 (CH, C-6 $\text{C}_6\text{H}_4\text{N}$), 138.3 (CH, C-4 $\text{C}_6\text{H}_4\text{N}$), 122.7 (CH, C-3 $\text{C}_6\text{H}_4\text{N}$), 122.2 (CH, C-5 $\text{C}_6\text{H}_4\text{N}$), 163.4 (qC, C-4 substituted Ph), 136.3 (qC, C-1 substituted Ph), 129.3 (2CH, C-2 substituted Ph), 113.2 (2CH, C-3 substituted Ph), 146.2 (qC, C-1 Ph), 128.0 (2CH, C-3 Ph), 127.8 (2CH, C-2 Ph), 127.2 (CH, C-4 Ph), 88.1 (qC, COH), 55.2 (OCH_3); M^+ (APCI, m/z): calculated 291.1259 ($\text{C}_{19}\text{H}_{17}\text{NO}_2$), found 291.1219 ($\text{C}_{19}\text{H}_{17}\text{NO}_2$), 274.1223 ($\text{C}_{19}\text{H}_{16}\text{NO}$), 184.0735 ($\text{C}_{13}\text{H}_{12}\text{O}$); IR (neat): $\nu(\text{OH}) = 3403 \text{ cm}^{-1}, \nu(\text{C-H, aromatic}) = 3059 \text{ cm}^{-1}, 3014 \text{ cm}^{-1}, 842 \text{ cm}^{-1}, \nu(\text{C-H, aliphatic}) = 2962 \text{ cm}^{-1}, 2930 \text{ cm}^{-1}, 2905 \text{ cm}^{-1}, 2833 \text{ cm}^{-1}, \nu(\text{C=C \& N=C, aromatic}) = 1614 \text{ cm}^{-1}, 1587 \text{ cm}^{-1}, 1569 \text{ cm}^{-1}, 1510 \text{ cm}^{-1}, \nu(\text{C-O, aliphatic}) = 1167 \text{ cm}^{-1}, 1027 \text{ cm}^{-1}, \nu(\text{C-O, phenol}) = 1248 \text{ cm}^{-1}.$

3.3.2. General Procedure for the Synthesis of the Lithium Salts 9–12

To the pyridinyl alcohol (2 mmol) in a Schlenk tube under argon atmosphere was added THF (20 mL). The alcohol was made to dissolve; $n\text{BuLi}$ (2 mmol, 2.5 M in hexane) was added drop-wise, and the reaction mixture was stirred for 2 h, at room temperature. The solvent was removed under reduced pressure, and the white solid residue obtained was washed with pentane (5 mL \times 2). The pentane was removed by gastight syringe, and the white solid was made to dry under reduced pressure. The white powder lithium salt was kept under inert atmosphere in a fridge for the next reaction.

3.3.3. General Procedure for the Synthesis of Complexes 4 and 13–15

The lithium salt of pyridin-2-yl-methanol (0.6 mmol, in 5 mL THF) was added to a Schlenk tube containing Grubbs second generation catalyst (0.6 mmol, in 5–10 mL THF) under inert atmosphere. The reaction mixture was stirred for 2–53 h at room temperature to 40 °C, depending on the reaction rate. Progress of the reaction was followed by TLC (thin layer chromatography) (6:1 hexane:ethyl acetate) until all of the Grubbs catalyst was consumed. The THF was removed from the resulting dark-green Grubbs 2-type precatalysts under reduced pressure in an inert condition. Toluene (7 mL) was added to the tarry black residue in the Schlenk tube, and all of the contents of the Schlenk tube were collected by gastight syringe and filtered into another Schlenk tube using a syringe filter, in an inert condition. Toluene was removed under reduced pressure; THF (1 mL) and pentane (5–10 mL) were added to the tarry black residue in the Schlenk tube, and the mixture was left for 20–30 min to form a precipitate. The pentane was removed by gastight syringe, and the product was washed with pentane (5 mL) using an ultrasonic bath for 5 min once and then four times without the ultrasonic

bath. The washed pentane was removed by a gastight syringe, and the final product was dried under reduced pressure in an inert condition.

Benzylidene-chloro(1,3-bis-(2,4,6-trimethylphenyl)-2-imidazolidinylidene)-[1-(2'-pyridinyl)-1,1-diphenyl-methanolato]ruthenium, **4**: Yield 0.458 g, 98%, green powder, dec.p. (decomposition point): 114 °C, $^1\text{H NMR}$ (CDCl_3 , 600 MHz, CDCl_3): $\delta_{\text{H}} = 17.10$ (s, 1H, carbene), 9.61 (d, 1H, $J = 5.48$ Hz, H-6 of $\text{C}_5\text{H}_4\text{N}$), 7.62 (t, 1H, $J = 7.58$ Hz, H-4 of $\text{C}_5\text{H}_4\text{N}$), 7.31–7.19 (m, 11H, H-3 of $\text{C}_5\text{H}_4\text{N}$ & all H's of 2Ph), 7.17–7.06 (m, 6H, all H's of carbene Ph & H-5 of $\text{C}_5\text{H}_4\text{N}$), 6.64 (s, 4H, H-3 of mesityl), 3.99 (m, 4H, H of $\text{N}(\text{CH}_2)_2\text{N}$), 2.61/2.27/2.19 (3s, 18H, 6 CH_3 of mesityl); $^{31}\text{P NMR}$ (CDCl_3 , 242 MHz): no signal; M^+ (MALDI, m/z): calculated 793.2372 ($\text{C}_{46}\text{H}_{46}\text{ClN}_3\text{ORu}$), found 793.2362 ($\text{C}_{46}\text{H}_{46}\text{ClN}_3\text{ORu}$). IR (neat): $\nu(\text{C-H, aromatic}) = 3055\text{ cm}^{-1}$, 3019 cm^{-1} , 760 cm^{-1} , $\nu(\text{CH}_3) = 2921\text{ cm}^{-1}$, 2849 cm^{-1} , 1379 cm^{-1} , $\nu(\text{C=N, \& C=C, aromatic}) = 1592\text{ cm}^{-1}$, 1568 cm^{-1} , $\nu(\text{C-N}) = 1262\text{ cm}^{-1}$, $\nu(\text{C-O, aliphatic}) = 1165\text{ cm}^{-1}$, 1024 cm^{-1} ; $^{13}\text{C NMR}$ (CDCl_3 , 150 MHz): $\delta_{\text{C}} = 291.70$, 214.44, 171.21, 151.55, 149.88, 149.75, 143.58, 139.21, 137.32, 136.62, 133.94, 129.63, 128.84, 128.39, 127.89, 126.97, 126.84, 126.58, 126.29, 126.11, 122.39, 120.94, 93.94, 51.33, 20.95, 19.07, 18.89.

Benzylidene-chloro(1,3-bis-(2,4,6-trimethylphenyl)-2-imidazolidinylidene)-[1-(2'-pyridinyl)-1-(2'-chlorophenyl)-1-phenyl-methanolato]ruthenium, **13**: Yield 0.33 g, 66%, light green powder, dec.p.: 210 °C, $^1\text{H NMR}$ (CDCl_3 , 600 MHz, CDCl_3): $\delta_{\text{H}} = 17.34/17.26$ (2s, 1H, carbene H), 9.76 (d, 1H, $J = 5.47$ Hz, H-6 of $\text{C}_5\text{H}_4\text{N}$), 7.65 (t, 1H, $J = 7.37$ Hz, H-4 of $\text{C}_5\text{H}_4\text{N}$), 7.36–7.40 (m, 4H, H of carbene Ph), 7.32 (t, 2H, $J = 7.89$ Hz, H-4 of carbene Ph & 5-H of $\text{C}_5\text{H}_4\text{N}$), 7.27 (d, 1H, $J = 7.89$ Hz, 3-H of $\text{C}_5\text{H}_4\text{N}$), 7.19–7.25 (m, 6H, H of unsubstituted Ph & 6-H of substituted Ph), 7.09 (m, 3H, 3-, 4- & 5-H of substituted Ph), 6.79–6.88 (2d, 4H, $J = 7.88$ Hz, H-3 of mesityl), 3.96 (m, 4H, $\text{N}(\text{CH}_2)_2\text{N}$), 2.65/2.52/2.21/2.14 (4s, 18H, 6 CH_3); $^{31}\text{P NMR}$ (CDCl_3 , 242 MHz): no signal; M^+ (MALDI, m/z): calculated 827.1983 ($\text{C}_{46}\text{H}_{45}\text{Cl}_2\text{N}_3\text{ORu}$), found 827.1972 ($\text{C}_{46}\text{H}_{45}\text{Cl}_2\text{N}_3\text{ORu}$); IR (neat): $\nu(\text{C-H, aromatic}) = 3057\text{ cm}^{-1}$, 3020 cm^{-1} , 756 cm^{-1} , $\nu(\text{CH}_3) = 2918\text{ cm}^{-1}$, 2853 cm^{-1} , $\nu(\text{C=N \& C=C, aromatic}) = 1627\text{ cm}^{-1}$, 1591 cm^{-1} , 1568 cm^{-1} , $\nu(\text{C-N, aliphatic}) = 1263\text{ cm}^{-1}$, $\nu(\text{C-O, aliphatic}) = 1162\text{ cm}^{-1}$, 1026 cm^{-1} ; $^{13}\text{C NMR}$ (CDCl_3 , 150 MHz): $\delta_{\text{C}} = 292.70$, 214.17, 171.86, 150.01, 149.84, 148.01, 138.87, 137.53, 136.71, 134.30, 131.05, 130.69, 129.45, 129.42, 128.96, 128.58, 127.31, 127.27, 126.95, 126.90, 126.43, 126.27, 125.16, 123.31, 121.16, 94.31, 51.51, 20.94, 18.93, 18.80.

Benzylidene-chloro(1,3-bis-(2,4,6-trimethylphenyl)-2-imidazolidinylidene)-[1-(2'-pyridinyl)-1-(4'-chlorophenyl)-1-phenyl-methanolato]ruthenium, **14**: Yield 0.46 g, 94%, light green powder, dec.p.: 88 °C, $^1\text{H NMR}$ (CDCl_3 , 600 MHz, CDCl_3): $\delta_{\text{H}} = 17.11/17.09$ (2s, 1H, carbene H), 9.55–9.70 (2d, 1H, $J = 5.32$ Hz, 6-H of $\text{C}_5\text{H}_4\text{N}$), 7.63 (t, 1H, $J = 7.56$ Hz, 4-H of $\text{C}_5\text{H}_4\text{N}$), 7.20–7.30 (m, 11H, 3-H of $\text{C}_5\text{H}_4\text{N}$, 2Ph), 7.15 (t, 2H, $J = 7.28$ Hz, meta-H of para-ClPh), 7.09 (t, 1H, $J = 7.56$ Hz, 5-H of $\text{C}_5\text{H}_4\text{N}$), 7.02 (d, 2H, $J = 8.12$ Hz, ortho-H of para-ClPh), 6.97/6.75 (2d, 4H, $J = 8.12$ Hz, mesityl H), 3.98 (m, 4H, $\text{N}(\text{CH}_2)_2\text{N}$), 2.60/2.28–2.19 (3s, 18H, 6 CH_3); $^{31}\text{P NMR}$ (CDCl_3 , 242 MHz): no signal; M^+ (ESI, m/z): calculated 827.1983 ($\text{C}_{46}\text{H}_{45}\text{Cl}_2\text{N}_3\text{ORu}$), found 827.1978 ($\text{C}_{46}\text{H}_{45}\text{Cl}_2\text{N}_3\text{ORu}$); IR (neat): IR: $\nu(\text{C-H, aromatic}) = 3055\text{ cm}^{-1}$, 3019 cm^{-1} , 817 cm^{-1} , $\nu(\text{CH}_3) = 2920\text{ cm}^{-1}$, 2848 cm^{-1} , $\nu(\text{C=N \& C=C, aromatic}) = 1589\text{--}1444\text{ cm}^{-1}$, $\nu(\text{C-N, aliphatic}) = 1260\text{ cm}^{-1}$, $\nu(\text{C-O, aliphatic}) = 1164\text{ cm}^{-1}$, 1090 cm^{-1} ; $^{13}\text{C NMR}$ (CDCl_3 , 150 MHz): $\delta_{\text{C}} = 292.35$, 214.20, 170.84, 151.41, 149.19, 143.26, 139.15, 137.52, 137.37, 129.80, 129.67, 129.25, 128.93, 128.31, 126.97, 126.92, 126.78, 126.60, 126.52, 126.32, 122.27, 121.14, 92.72, 51.31, 20.95, 19.09, 18.85.

Benzylidene-chloro(1,3-bis-(2,4,6-trimethylphenyl)-2-imidazolidinylidene)-[1-(2'-pyridinyl)-1-(4'-methoxyphenyl)-1-phenyl-methanolato]ruthenium, **15**: Yield 0.46 g, 95.8%, dark green powder, dec.p.: 73.5 °C, $^1\text{H NMR}$ (CDCl_3 , 600 MHz, CDCl_3): $\delta_{\text{H}} = 17.10/17.08$ (2s, 1H, carbene-H), 9.63–9.60 (2d, 1H, $J = 5.74$ Hz, H-6 of $\text{C}_5\text{H}_4\text{N}$), 7.61 (t, 1H, $J = 7.74$ Hz, H-4 of $\text{C}_5\text{H}_4\text{N}$), 7.11–7.28 (m, 12H, 3-, 5-H of $\text{C}_5\text{H}_4\text{N}$, & all H of 2Ph), 7.08 (d, 2H, $J = 8.16$ Hz, H-2 & H-6 of substituted Ph), 6.94 (m, 2H, H-3 & H-5 of substituted Ph), 6.73–6.81 (2d, 4H, $J = 8.55$ Hz, mesityl-H), 4.01 (m, 4H, $\text{N}(\text{CH}_2)_2\text{N}$), 3.77 (s, 3H, OCH_3), 2.62/2.28/2.20 (3s, 18H, 6 CH_3 of mesityl); $^{31}\text{P NMR}$ (CDCl_3 , 242 MHz): no signal; M^+

(ESI, m/z): calculated 823.2478 ($C_{47}H_{48}ClN_3O_2Ru$), found 823.2407 ($C_{47}H_{48}ClN_3O_2Ru$); IR (neat): $\nu(\text{C-H, aromatic}) = 3055\text{ cm}^{-1}$, 3017 cm^{-1} , 828 cm^{-1} , $\nu(\text{CH}_3) = 2927\text{ cm}^{-1}$, 2851 cm^{-1} , $\nu(\text{C=N \& C=C, aromatic}) = 1606\text{ cm}^{-1}$, 1590 cm^{-1} , 1507 cm^{-1} , $\nu(\text{C-N, aliphatic}) = 1245\text{ cm}^{-1}$, $\nu(\text{C-O, aliphatic}) = 1164\text{ cm}^{-1}$, 1029 cm^{-1} , $\nu(\text{C-O, phenol}) = 1297\text{ cm}^{-1}$; ^{13}C NMR (CDCl_3 , 150 MHz): $\delta_{\text{C}} = 291.16$, 214.47 , 171.48 , 151.50 , 149.87 , 139.23 , 137.20 , 136.63 , 135.74 , 133.92 , 129.65 , 128.85 , 128.44 , 126.94 , 126.83 , 126.59 , 126.37 , 126.28 , 126.24 , 120.88 , 112.30 , 92.77 , 55.23 , 51.32 , 20.95 , 19.09 , 18.90 .

3.4. Catalytic Reactions

A small-scale reactor (5 mL) was used for the 1-octene metathesis reactions. To this reactor, flushed with argon, the precatalysts and 1-octene were added in a 1:9000 molar ratio. Nonane (0.25 mL) was added as the internal standard; *tert*-BuOOH (2 drops) and toluene (0.3 mL) were added to quench the reaction and to increase the volume of the sample for GC analysis. Samples (0.05 mL) were collected at predetermined time intervals, and the progress of the reaction was monitored using an Agilent 6890 GC/FID (Gas Chromatograph equipped with a Flame Ionization Detector) (Agilent Technologies, Santa Clara, CA, USA).

3.5. Computational Details

All structures were optimized using the gradient corrected Perdew-Burke-Ernzerhof (PBE) [37] functional according to a previous work done by Minenkov et al. [38], Jacobsen [39] and Du Toit et al. [35]. Optimizations were run in DMol³, a DFT module of Accelrys Materials Studio 6.1 [33]. The double numerical basis set with a polarization p-function on the hydrogen atoms (DNP) was used for all complexes. Steric interaction between any atom/group of atoms in the complexes was calculated using Solid Angle [34]. The energy calculations were done based on previous work [35,40,41] also using the gradient corrected PBE [37] functional with the empirical D3 version of Grimme's dispersion with Becke-Johnson damping (PBE-D3(BJ)) [42]. For Ru, the Stuttgart 28-electron relativistic effective core potential (ECP28MDF) with accompanying correlation consistent polarized valence quadruple zeta (cc-pVQZ-PP) basis set was used [43]. Furthermore, for the C and H atoms, the correlation consistent polarized valence quadruple zeta (cc-pVQZ) [44,45] basis set was chosen; whereas, for the rest of the atoms, an extended cc-pVQZ basis set obtained by adding diffuse functions from the augmented cc-pVQZ diffuse (aug-cc-pVQZ diffuse) [45,46] basis set was used. All basis sets were obtained from the Environmental Molecular Sciences Laboratory (EMSL) basis set exchange website [47,48]. The solvent effect was calculated with the polarizable continuum solvation model (PCM) [49–52]. Electrostatic and non-electrostatic effects were calculated by including the "Dis", "Rep" and "Cav" Gaussian keywords with chlorobenzene as the solvent. For the solute cavity, the atomic radii was set to UAHF (united atom topological model for the Hartree-Fock level of theory). All properties were obtained from the Gaussian output files using the pop = NBOread keyword.

4. Conclusions

Four pyridinyl alcohols and four ruthenium-based precatalysts were successfully synthesized. The pyridinyl alcohol 1-(2'-pyridinyl)-1-(4-methoxyphenyl)-1-phenyl-methanol, the two chloro-substituted and the methoxy-substituted pyridinyl alcoholato ruthenium precatalysts were also synthesized for the first time. The very good performance of the 4-chloro- and 4-methoxy-substituted pyridinyl alcoholato ligand containing ruthenium precatalysts, at high temperatures, makes them very good precatalysts for high temperature linear olefin metathesis reactions. The significant increase in the catalytic performance of the newly-synthesized ruthenium precatalysts, at high temperatures, is attributed to the steric repulsions between the substituents and the sterically bulky NHC group that resulted in strengthening the Ru-N bond.

Acknowledgments: We are grateful to North-West University (NWU), the South African Department of Science and Technology-National Research Foundation's (DST-NRF) Centre of Excellence in Catalysis (c*change) for the financial support and Andre Joubert (NWU) for the acquisition of the NMR spectra.

Author Contributions: H.C.M.V., T.T.T. and J.H.L.J. conceived of and designed the experiments. T.T.T. performed the experiments. H.C.M.V., T.T.T. and J.H.L.J. analyzed the experimental data. J.I.d.T. and C.G.C.E.v.S. performed the modelling and analyzed the modelling data. H.C.M.V. contributed reagents/materials/analysis tools. T.T.T. wrote the paper.

Conflicts of Interest: The authors declare no conflict of interest. The founding sponsors had no role in the design of the study; in the collection, analyses or interpretation of data; in the writing of the manuscript; nor in the decision to publish the results.

References

1. Dias, E.L.; Nguyen, S.T.; Grubbs, R. Well-defined ruthenium olefin metathesis catalysts: Mechanism and activity. *J. Am. Chem. Soc.* **1997**, *119*, 3887–3897. [[CrossRef](#)]
2. Dinger, M.B.; Mol, J.C. High turnover numbers with ruthenium-based metathesis catalysts. *Adv. Synth. Catal.* **2002**, *344*, 671–677. [[CrossRef](#)]
3. Van Schalkwyk, C.; Vosloo, H.C.M.; du Plessis, J.A.K. A comparison of the activity of homogeneous tungsten and ruthenium catalysts for the metathesis of 1-octene. *Adv. Synth. Catal.* **2002**, *344*, 781–788. [[CrossRef](#)]
4. Grubbs, R.H. The development of functional group tolerant rump catalysts. *J. Macromol. Sci. Part A* **1994**, *31*, 1829–1933. [[CrossRef](#)]
5. Huang, J.; Schanz, H.-J.; Stevens, E.D.; Nolan, S.P. Influence of sterically demanding carbene ligation on catalytic behavior and thermal stability of ruthenium olefin metathesis catalysts. *Organometallics* **1999**, *18*, 5375–5380. [[CrossRef](#)]
6. Weskamp, T.; Kohl, F.J.; Hieringer, W.; Gleich, D.; Herrmann, W.A. Highly active ruthenium catalysts for olefin metathesis: The synergy of *n*-heterocyclic carbenes and coordinatively labile ligands. *Angew. Chem. Int. Ed.* **1999**, *38*, 2416–2419. [[CrossRef](#)]
7. Scholl, M.; Trnka, T.M.; Morgan, J.P.; Grubbs, R.H. Increased ring closing metathesis activity of ruthenium-based olefin metathesis catalysts coordinated with imidazolin-2-ylidene ligands. *Tetrahedron Lett.* **1999**, *40*, 2247–2250. [[CrossRef](#)]
8. Lehman, S.E.; Schwendeman, J.E.; O'Donnell, P.M.; Wagener, K.B. Olefin isomerization promoted by olefin metathesis catalysts. *Inorg. Chim. Acta* **2003**, *345*, 190–198. [[CrossRef](#)]
9. Maechling, S.; Zaja, M.; Blechert, S. Unexpected results of a turnover number (TON) study utilising ruthenium-based olefin metathesis catalysts. *Adv. Synth. Catal.* **2005**, *347*, 1413–1422. [[CrossRef](#)]
10. Meyer, W.H.; Brüll, R.; Raubenheimer, H.G.; Thompson, C.; Kruger, G.J. Thioethercarboxylates in palladium chemistry: First proof of hemilabile properties of S–O ligands. *J. Organomet. Chem.* **1998**, *553*, 83–90. [[CrossRef](#)]
11. Denk, K.; Fridgen, J.; Herrmann, W.A. N-heterocyclic carbenes, Part 33. Combining stable NHC and chelating pyridinyl-alcoholato ligands: A ruthenium catalyst for applications at elevated temperatures. *Adv. Synth. Catal.* **2002**, *344*, 666–670. [[CrossRef](#)]
12. Francis, J.A.; Bott, S.G.; Barron, A.R. Aluminium compounds containing bidentate ligands: Chelate ring size and rigid conformation effects. *J. Chem. Soc. Dalton Trans.* **1998**, 3305–3310. [[CrossRef](#)]
13. Slugovc, C.; Burtscher, D.; Stelzer, F.; Mereiter, K. Thermally switchable olefin metathesis initiators bearing chelating carbenes: Influence of the chelate's ring size. *Organometallics* **2005**, *24*, 2255–2258. [[CrossRef](#)]
14. van der Schaaf, P.A.; Kolly, R.; Kirner, H.-J.; Rime, F.; Mühlebach, A.; Hafner, A. Synthesis and reactivity of novel ruthenium carbene catalysts. X-ray structures of $[\text{RuCl}_2(\text{CHSC}_6\text{H}_5)(\text{P}^i\text{Pr}_3)_2]$ and $[\text{RuCl}_2(\text{CHCH}_2\text{CH}_2\text{-C}_N\text{-2-C}_5\text{H}_4\text{N})(\text{P}^i\text{Pr}_3)]$. *J. Organomet. Chem.* **2000**, *606*, 65–74. [[CrossRef](#)]
15. Kingsbury, J.S.; Harrity, J.P.; Bonitatebus, P.J.; Hoveyda, A.H. A recyclable Ru-based metathesis catalyst. *J. Am. Chem. Soc.* **1999**, *121*, 791–799. [[CrossRef](#)]
16. Garber, S.B.; Kingsbury, J.S.; Gray, B.L.; Hoveyda, A.H. Efficient and recyclable monomeric and dendritic Ru-based metathesis catalysts. *J. Am. Chem. Soc.* **2000**, *122*, 8168–8179. [[CrossRef](#)]
17. Gessler, S.; Randl, S.; Blechert, S. Synthesis and metathesis reactions of a phosphine-free dihydroimidazole carbene ruthenium complex. *Tetrahedron Lett.* **2000**, *41*, 9973–9976. [[CrossRef](#)]
18. Hoveyda, A.H.; Gillingham, D.G.; Van Veldhuizen, J.J.; Kataoka, O.; Garber, S.B.; Kingsbury, J.S.; Harrity, J.P. Ru complexes bearing bidentate carbenes: From innocent curiosity to uniquely effective catalysts for olefin metathesis. *Organ. Biomol. Chem.* **2004**, *2*, 8–23. [[CrossRef](#)] [[PubMed](#)]

19. Chang, S.; Jones, L.; Wang, C.; Henling, L.M.; Grubbs, R.H. Synthesis and characterization of new ruthenium-based olefin metathesis catalysts coordinated with bidentate schiff-base ligands. *Organometallics* **1998**, *17*, 3460–3465. [[CrossRef](#)]
20. De Clercq, B.; Verpoort, F. Activity of a new class of ruthenium based ring-closing metathesis and ring-opening metathesis polymerization catalysts coordinated with a 1, 3-dimesityl-4, 5-dihydroimidazol-2-ylidene and a schiff base ligand. *Tetrahedron Lett.* **2002**, *43*, 9101–9104. [[CrossRef](#)]
21. De Clercq, B.; Verpoort, F. A new class of ruthenium complexes containing Schiff base ligands as promising catalysts for atom transfer radical polymerization and ring opening metathesis polymerization. *J. Mol. Catal. A: Chem.* **2002**, *180*, 67–76. [[CrossRef](#)]
22. Van Der Schaaf, P.A.; Mühlebach, A.; Hafner, A.; Kolly, R. Heterocyclyl Ligand Containing Ruthenium and Osmium Catalysts. WO Patent 1999029701 A1, 24 November 1998.
23. Jordaan, M. Experimental and Theoretical Investigation of New Grubbs-Type Catalysts for the Metathesis of Alkenes. Ph.D. Thesis, North-West University, Potchefstroom, South Africa, 2007.
24. Du Toit, J.I.; Jordaan, M.; Huijsmans, C.A.A.; Jordaan, J.H.L.; van Sittert, C.G.C.E.; Vosloo, H.C.M. Improved metathesis lifetime: Chelating pyridinyl-alcoholato ligands in the second generation Grubbs precatalyst. *Molecules* **2014**, *19*, 5522–5537. [[CrossRef](#)] [[PubMed](#)]
25. De Klerk, A. Sasol 2 and 3 facilities. In *Fischer-Tropsch Refining*; Wiley-VCH: Weinheim, Germany, 2011; pp. 181–212.
26. Tole, T.T.; Jordaan, J.H.L.; Vosloo, H.C.M. Synthetic methods of α -pyridinyl and α -bipyridinyl alcohols and α, α' -pyridine and α, α' -bipyridine diols. *Curr. Organ. Synth.* **2015**, *12*, 261–304. [[CrossRef](#)]
27. Herrmann, W.A.; Lobmaier, G.M.; Priermeier, T.; Mattner, M.R.; Scharbert, B. New dioxomolybdenum (VI) catalysts for the selective oxidation of terminal *n*-alkenes with molecular oxygen. *J. Mol. Catal. A: Chem.* **1997**, *117*, 455–469. [[CrossRef](#)]
28. Sperber, N.; Papa, D.; Schwenk, E.; Sherlock, M. Pyridyl-substituted alkamine ethers as antihistaminic agents. *J. Am. Chem. Soc.* **1949**, *71*, 887–890. [[CrossRef](#)] [[PubMed](#)]
29. McCarty, F.J.; Tilford, C.H.; Van Campen, M., Jr. Central stimulants. α, α -Disubstituted 2-piperidinemethanols and 1,1-disubstituted heptahydroöxazolo [3, 4-a] pyridines. *J. Am. Chem. Soc.* **1957**, *79*, 472–480. [[CrossRef](#)]
30. Silverstein, R.M.; Webster, F.X.; Kiemle, D.; Bryce, D.L. Infrared spectroscopy. In *Spectrometric Identification of Organic Compounds*, 8th ed.; Wiley: Chichester, UK, 2015; pp. 71–125.
31. Van der Gryp, P.; Barnard, A.; Cronje, J.-P.; de Vlieger, D.; Marx, S.; Vosloo, H.C.M. Separation of different metathesis grubbs-type catalysts using organic solvent nanofiltration. *J. Membr. Sci.* **2010**, *353*, 70–77. [[CrossRef](#)]
32. Ritter, T.; Hejl, A.; Wenzel, A.G.; Funk, T.W.; Grubbs, R.H. A standard system of characterization for olefin metathesis catalysts. *Organometallics* **2006**, *25*, 5740–5745. [[CrossRef](#)]
33. Accelrys Software Inc. *Materials Studio Release Notes, Release 6.1*; Accelrys Software Inc.: San Diego, CA, USA, 2012.
34. Guzei, I.A.; Wendt, M. An improved method for the computation of ligand steric effects based on solid angles. *Dalton Trans.* **2006**, 3991–3999. [[CrossRef](#)] [[PubMed](#)]
35. Du Toit, J.I.; van Sittert, C.G.C.E.; Vosloo, H.C.M. Towards a better understanding of alkene metathesis: Elucidating the properties of the major metal carbene catalyst types. *Monatshfte Chem.-Chem. Mon.* **2015**, *146*, 1115–1129. [[CrossRef](#)]
36. Wiberg, K.B. Application of the Pople-Santry-Segal CNDO method to the cyclopropylcarbinyl and cyclobutyl cation and to bicyclobutane. *Tetrahedron* **1968**, *24*, 1083–1096. [[CrossRef](#)]
37. Perdew, J.P.; Burke, K.; Ernzerhof, M. Generalized gradient approximation made simple. *Phys. Rev. Lett.* **1996**, *77*, 3865–3868. [[CrossRef](#)] [[PubMed](#)]
38. Minenkov, Y.; Singstad, A.; Occhipinti, G.; Jensen, V.R. The accuracy of DFT-optimized geometries of functional transition metal compounds: A validation study of catalysts for olefin metathesis and other reactions in the homogeneous phase. *Dalton Trans.* **2012**, *41*, 5526–5541. [[CrossRef](#)] [[PubMed](#)]
39. Jacobsen, H. Hydrogen and dihydrogen bonding of transition metal hydrides. *Chem. Phys.* **2008**, *345*, 95–102. [[CrossRef](#)]
40. Minenkov, Y.; Occhipinti, G.; Jensen, V.R. Complete reaction pathway of ruthenium-catalyzed olefin metathesis of ethyl vinyl ether: Kinetics and mechanistic insight from DFT. *Organometallics* **2013**, *32*, 2099–2111. [[CrossRef](#)]

41. Occhipinti, G.; Koudriavtsev, V.; Törnroos, K.W.; Jensen, V.R. Theory-assisted development of a robust and z-selective olefin metathesis catalyst. *Dalton Trans.* **2014**, *43*, 11106–11117. [[CrossRef](#)] [[PubMed](#)]
42. Grimme, S.; Ehrlich, S.; Goerigk, L. Effect of the damping function in dispersion corrected density functional theory. *J. Comput. Chem.* **2011**, *32*, 1456–1465. [[CrossRef](#)] [[PubMed](#)]
43. Peterson, K.A.; Figgen, D.; Dolg, M.; Stoll, H. Energy-consistent relativistic pseudopotentials and correlation consistent basis sets for the 4d elements Y–Pd. *J. Chem. Phys.* **2007**, *126*, 124101. [[CrossRef](#)] [[PubMed](#)]
44. Dunning, T.H. Gaussian basis sets for use in correlated molecular calculations. I. The atoms boron through neon and hydrogen. *J. Chem. Phys.* **1989**, *90*, 1007–1023. [[CrossRef](#)]
45. Woon, D.E.; Dunning, T.H. Gaussian basis sets for use in correlated molecular calculations. III. The atoms aluminum through argon. *J. Chem. Phys.* **1993**, *98*, 1358–1371. [[CrossRef](#)]
46. Kendall, R.A.; Dunning, T.H.; Harrison, R.J. Electron affinities of the first-row atoms revisited. Systematic basis sets and wave functions. *J. Chem. Phys.* **1992**, *96*, 6796–6806. [[CrossRef](#)]
47. Feller, D. The role of databases in support of computational chemistry calculations. *J. Comput. Chem.* **1996**, *17*, 1571–1586. [[CrossRef](#)]
48. EMSL Basis Set Exchange v1.2.2. Available online: <https://bse.pnl.gov/bse/portal> (accessed on 4 July 2016).
49. Tomasi, J.; Persico, M. Molecular interactions in solution: An overview of methods based on continuous distributions of the solvent. *Chem. Rev.* **1994**, *94*, 2027–2094. [[CrossRef](#)]
50. Tomasi, J.; Mennucci, B.; Cammi, R. Quantum mechanical continuum solvation models. *Chem. Rev.* **2005**, *105*, 2999–3094. [[CrossRef](#)] [[PubMed](#)]
51. Cossi, M.; Scalmani, G.; Rega, N.; Barone, V. New developments in the polarizable continuum model for quantum mechanical and classical calculations on molecules in solution. *J. Chem. Phys.* **2002**, *117*, 43–54. [[CrossRef](#)]
52. Scalmani, G.; Frisch, M.J. Continuous surface charge polarizable continuum models of solvation. I. General formalism. *J. Chem. Phys.* **2010**, *132*, 114110–114115. [[CrossRef](#)] [[PubMed](#)]



© 2017 by the authors; licensee MDPI, Basel, Switzerland. This article is an open access article distributed under the terms and conditions of the Creative Commons Attribution (CC-BY) license (<http://creativecommons.org/licenses/by/4.0/>).